DOCTORAL DISSERTATION

DEVELOPMENT AND CONTROL OF ROBOTIC CANES FOR WALKING ASSISTANCE

(歩行支援用ロボット杖の開発と制御)

Graduate School of Engineering

Yokohama National University

PHI VAN LAM

September 2019

DECLARATION

I hereby proclaim that I am the sole creator of this bona fide dissertation entitled *"Development and Control of the Robotic Canes for Walking Assistance"*. This is a true copy of the thesis, including all required revisions, as accepted by the review Committee Members.

I hereby consent to this doctoral dissertation being registered and published in the YNU Repository in accordance with the YNU Repository Guidelines. I also consent to the National Library receiving a copy of the published file from the YNU Repository for the purpose aechiving and providing it for public viewing within the library facilities.

I hereby comfirm that the details quoted or reprnted within the doctoral dissertation are not in violation of the Copyright Atc.

Phi Van Lam

Members of Ph.D. Dissertation Committee:

- Prof. Yasutaka Fujimoto, *Yokohama National University.*
- Prof. Tomoyuki Shimono, *Yokohama National University.*
- Prof. Takao Tsuji, *Yokohama National University.*
- Prof. Koichi Ichige, *Yokohama National University.*
- Prof. Tsutomu Oyama, *Yokohama National University.*

ABSTRACT

This research highlights the control method and analysis of robotic canes for walking assistance. It focuses on improving the performance of the previous studies about the nonlinear controller systems, the linearization of the nonlinear system by utilizing the Lie algebra method (LAM) and the nonlinear disturbance observer (NDOB) in the real models. Originating from the simulation model and the incomplete hardware design of a robotic cane which was studied for walking assistance with an omnidirectional wheel built on an inverted pendulum model by Mr. Kyohei Shimizu [25–28], we have developed and fabricated this robotic cane with a perfect hardware design and expected abilities like high stability, self-balance, help for standing and walking and prevention of fall. Moreover, this cane is extremely safe for the user thanks to the mechatronic safety part mounted on the robotic cane. The weight of the robotic cane is also considered, especially the battery weight with smart functions for walking support.

Next, the NDOB proposed by Dr. Issam Abed Smadi [29] is considered a strongly effective solution to guarantee global exponential stability for robot manipulators. Its eficiency was proved by simulation results on a monowheel robot model. But, the performance of the NDOB have not been verified on any specific hardware yet. With the above advantages, the NDOB is thoroughly utilized to determine the external force acting on the rod of the robotic canes, then, to control the behaviors of the robotic canes to support the user in maintaining balance depending on the user behaviors in the real model. A method of the smart mode switching for the nonlinear controller is proposed in this study by changing gains of the controller according to the change of the external force acting on the rod of the robotic canes by using the NDOB results. Eperimental results of this method on the real model of the robotic canes indicate that the robotic canes can truely support the user for walking assistance more conveniently than the previously proposed methods. The performance evaluation of the controller is verified on both the simulation results and the real experimental results of the robotic canes for walking assistance on different environments. To improve the performance of the robotic canes in support blind people, the image processing method is applied to the system to determine the navigated lines of the blind people to support them to walk by color detection algorithms. The initial results of the method on the robotic canes show that the robotic canes become more effective to support the blind people to walk in

unknown environments.

Besides, the efficiency of the LAM is also compared with that of a traditional control algorithm -the linear quadratic regulator (LQR). The low-pass filter is designed to be set to the input signals of the nonlinear controller of the robotic canes to eliminate noises in the actual model in practice. By combining the smart mode switching with the low-pass filter, the robotic canes can work more smoothly, and therefore, the user feel more comfortable while they are using the robotic cane.

In order to expand the direction of research, the reliability of the proposed method is test successfully on the hardware of two modified new robotic canes with in-wheel brushless motors: two-wheeled cane and two-wheeled walker. The evaluation of the performance of the methods applied to the actual model of the robotic canes is carried out on a variety of objects and different working environments give equally good results in walking assistance functions. The robotic canes are expected as one of the smart walking assistance devices to support the older or the disabled including the blind in the future of our smart society.

ACKNOWLEDGMENTS

The research in this dissertation could not been completed if there are not the assistance, the patience and the support of many individuals.

I would like to express my sincere gratitude to my supervisor - Prof. Yasutaka Fujimoto for having accepted me in his laboratory as a research student, a doctoral student, and giving me great opportunities, motivating ideas and invaluable advice. In additions, I would like to thank review committee members for their valuable advice and guidance.

I am very grateful to the Otsuka Toshimi Scholarship Foundation for the award of Otsuka scholarship and the Vietnamese government through the University of Transport and Communications for giving me the opportunity to study this doctoral course. I would like to give many thanks to all of Fujimoto lab members for unconditional support such as Cyusa S. Christophe, Kenta Nagano. Especially, I want to thank Kyohei Shimizu for his support in the process of designing and producing a basic prototype that is a prerequisite for success of my research.

I would also like to thank my wife - Tran Thi Lan, who always stand by me in the most difficult time and give me continuous encouragements throughout this experience. To my beloved daughter - Phi Gia Linh, who always makes me happy when I return home after a hard working day. You are the love of my life.

Finally, I am thankful to my parents Phi Van Xuan and Nguyen Thi Them without whose love, support, and understanding I would never have finished this doctoral course. I always remember and head to you wherever I go in my life.

"You can do it If you think you can"
Phi Van Lam

Phi Van Lam
Yokohama, Japan
September 2019

Table of Contents

List of Tables

List of Figures

Chapter 1

Introduction

1.1 Motivation

Population worldwide has witnessed considerable aging in both quantity and age. The number of elderly people is 524 million in 2010, and is estimated to be nearly 1.5 billion in 2050 [30]. Caring the elder people become a serious problem in the modern society. Walking assistant devices play a crucial role to solve this issue.

There are wearable support devices proposed in [4, 11, 12, 15, 16, 32] to help elderly and the handicapped to walk and stand. But, they are quite complicated, and users need to wear them like wearing on the leg joints, which is awkward for the users, and sometimes they may be dangerous for the users because connections between these devices and the user are not being free. In this way, they are reasonable just in some assigned restoration focuses and are incapable in the daily life of the users.

A different kind of support device is clever wheelchairs [9, 33]. The users can be supported by sitting on the wheelchair. These wheelchairs are suitable for the users who can not move properly. Be that as it may, they are awkward and require a huge working space. They may likewise require around an extra supporter to work them. In this manner, savvy wheelchairs are constrained to indoor use or to recovery focuses or medical clinic where extra partners are accessible. More convenience assistance robots was proposed in [5,17]. By using the grip handle, the robots can support the user to walk or stand. However, like wheelchair devices, these devices are bulky, need a large maneuvering working space, and require additional operators. Moreover, their use is limited to working environments as flat surfaces.

A robotic cane utilizing three omnidirectional wheels to support the user to walk with the motion position controller has been proposed in [20]. This robotic cane can not only turn easily but also has a fall prevention function which is expected for any walking assistance devices. However, the hardware design is not so much convenient as remains bulky and complicated.

The application of the omnidirectional wheel structure for robotic canes in [20] was developed in [25–28]. However, the performance of these canes were only checked in simulation results without any experimental results on real devices. Especially, the authors in [22] had a patent for their robotic cane design without experimental results but it can open many new directions for the development of designs later. The benefit of the omnidirectional wheel is more compact than the omnidirectional ball robot in [31] or the three omni-wheeled cane robot in [20], and significantly reduces the size of the robotic cane, which is very essential with the walking assistance devices.

1.2 Objectives

Coming from the above-mentioned motivations, this study will solve problems of previous researches as follows: Firstly, this thesis presents a robotic cane that aid the users to keep up their balance, while addressing the weak points of the previous designs. The robotic cane utilizes an extraordinarily planned shrewd omnidirectional wheel, presenting both conservativeness and adaptability and lightweight. Next, in order to tackle the disadvantages from the above mentioned researches, a two-wheel cane based on two natural rubber tire electric wheels is also proposed in this thesis. Parallel with the hardware design of the robot model and the controller, the actual test results with the users are obtained. Moreover, in order to make a more convenient device to support the older or elderly people to stand or to walk indoor or outdoor environments, we also design a two-wheeled walker with the U-shape special structure. The performance of this device also proves by very good experimental results on a real robot in the real environments.

Finally, make more support to the blind people to walk, we propose an image processing method to determine the navigate line to control the motion of the robotic cane to help the blind people to easily walk and keep up balance.

The design of the robotic canes is based on an inverted pendulum model linearized by the LAM. The human external force applied to the robotic canes is estimated by the NDOB also proposed. To make the convenient interaction between the users and the robotic canes we use smooth mode switching method to change the modes of the controller to control the robotic canes based on the behavior of the users.

A basic inverted pendulum model of a traditional mechanical system has developed in this study. In the previous studies, the steadiness of the inverted pendulum model was controlled by variety of different methods: basic control loop feedback [23]; fuzzy-logic controller [1, 18]; a linear quadratic regulator (LQR) [13, 14]; additional sliding-mode control (SMC) [2, 6]; newton networks [21, 24], and a new NDOB [7]. The authors [10, 19] controlled the position and the velocity of a popular inverted pendulum model by using two new controllers. The installed controllers maintain a strong and stable position of the robot at the desired simulation point, but the effectiveness of the controllers are not examined in real model. In [3], the authors have regulated the torque and the velocity of an inverted pendulum motor in an analytical simulation study, and describe trade-offs between control methods in different application cases.

All of the previous studies just focused on the stability of the inverted pendulum around the equilibrium point as around the zero degree. However, these stability only around the equilibrium point are not enough for practical applications or for walking assistance. The proposed robotic canes in this study can solve this problem. They have a high stability with much bigger angle. To support the user to walk, walking assistance robots need a strong stability far from the zero position. This thesis resolves the equilibrium problem through the LAM and the NDOB with the balancing point not only around zero degrees as the popular methods. The LAM is directly administered to the nonlinear controller. The LAM can linearize the nonlinear system of the robotic canes even the balancing angle largely deviates from the equilibrium point. Meanwhile, the NDOB estimates the user's external force applied to the robotic canes to control the motion of the robotic canes depending on the user behaviors. As a result, the robotic canes are provided with a fall prevention function so that the users can be not fallen forward or falling to backward when used the robotic canes to walk or to stand. This function is a strongly expected point of any walking assistance devices.

The author in [29] has presented the NDOB in detail and achieved the simulation results of a mono-wheel robot model. Like studies in [25–28], the execution of the NDOB in [29] is proved on simulation models. Besides, it shows complexity and the inability to apply to practical applications. Because of that, it need to be developed. When applying the LAM and NDOB into my robotic canes application model, I had to develop it in the form of adding an intelligent mode switch to the central controller to be able to meet the application of the robotic canes for walking assistance.

The hardware design of the robotic canes is completed to assist the user to keep up steadiness. Especially, the controller is fabricated with high precision, high-rate processing and optimal parameters. We experimentally prove a high stability and quick responses of the canes to the behavior of users. Furthermore, the LAM is more consistent in self-standing modes than the LQR conventional technique, which creates a few vibrations. In particular, if the users intend to fall backward or to fall forward, the robotic canes rapidly reestablish their equilibrium point. Many positive feedbacks are received from elderly and disabled. The robotic canes are also passed the electromagnetic compatibility test. This proves that they are safe for human bodies.

1.3 Thesis Chapterization

This section presents the organization of this thesis which consists of six chapters as follows:

- Chapter 1 - Introduction
- Chapter 2 - Hardware design of the robotic cane
- Chapter 3 - Mathematical model and controller of the robotic cane
- Chapter 4 - Performance evaluation of the robotic cane

- Chapter 5 - Extended experiment results on the two-wheeled cane and the two-wheeled walker.

- Chapter 6 - Conclusion.

In the Chapter 1, we introduce the motivations and objectives of this research. Chapter 2 presents hardware of the robotic canes in this study in detail while Chapter 3 discusses mathematical models and control algorithms of the robotic canes. The performance of the one-wheel robotic cane is shown in Chapter 4 by both simulation results and experiment results on a real model. Next, extended experiment results on two another robotic canes which are developed based on the one-wheel robotic cane in Chapter 4 are presented. In addition, image processing is applied to the robotic canes to aid the blind to determine the navigate line while walking. Finally, a summary of this study is provided in Chapter 6.

Chapter 2

Complete Hardware of the Robotic Canes

2.1 Abstract

Taking advantage of omnidirectional wheel form of the robotic cane in [20], researchers have developed some robotic canes with this form in [25–28]. However, their methods were checked in simulation models rather than on practical hardware for real use. The authors in [22] were patented thanks to their designed robotic cane without experiment verification. But, it opens many new directions for the development of this type of the robotic cane. The special omnidirectional wheel is more concise than the omnidirectional ball in [31] or the three Omni-wheeled cane robot in [20]. The size of the robotic cane which is very important with any walking assistance device is well miniaturized in this study.

This chapter analyzes the hardware design of the robotic canes for walking assistance built on an inverted pendulum form. Whether the control algorithm can be successful or not is highly decided by whether the hardware design is good or not.In order to aid users to keep up balance in practical use, the hardware design has to be considered carefully.

This section details the structure of the robotic cane which was introduced in [25-28] for walking assistance. The basic prototype of the robotic cane is based on omnidirectional wheel and is controlled by a PC without any battery and emergency safety structure to protect the user. In this study, it is developed with a complete design of the robotic cane with high speed controller

based on Raspberry Pi Model B+ as a center controller and emergency safety structure by using ratchet mechanic structure. Battery and sensors are added to provide more functions for the robotic cane.

Moreover, two new designs which are developed from the one-wheeled robotic cane: a two-wheeled cane and two-wheeled walker for walking assistance are also presented. These canes are equipped with in-wheel motors with the fast response to the user behavior and a safe power.

All of the robotic canes designed has success with several tests on the users.

2.2 Complete Hardware of the Robotic Cane

This section discusses the complete hardware of the robotic cane in detail.

Fig. 2.1 shows a overview structure of the robotic cane (one-wheel cane). The robotic cane consists of a gyroscope sensor, a grip handle and a rod. It has a battery protection module including a LED display that shows the temperature, the voltage, and the current of the external battery, an on/off power switches and an emergency switch. The battery protection module can measure and control the output power supply to the robotic cane. When the used current is high or the batteries cell is hot, this protection board will interrupt immediately the output power to protect the battery not being broken. The working modes and smooth mode switching of the robotic cane is controlled and adjusted by using a touch sensor mounted on the top of the grip handle.

The special structure of the gearbox uses an omnidirectional wheel (Fig. 2.2). The robotic cane is able to turn to the left or right thanks to the lateral wheels, and go to backward or forward on the sagittal wheel. Directional rotations make an omnidirectional reply to the velocity and directions of the two brushless motors. Inverse rotation directions of the two Scorpion brushless motors provoke left-right motions of the lateral wheels. Inversely, when these two motors turn in the similar direction, the sagittal wheel rotates around the motor axis. Therefore, the robotic cane can be steered in any direction following the velocity and rotation directions of the two Scorpion brushless motors.

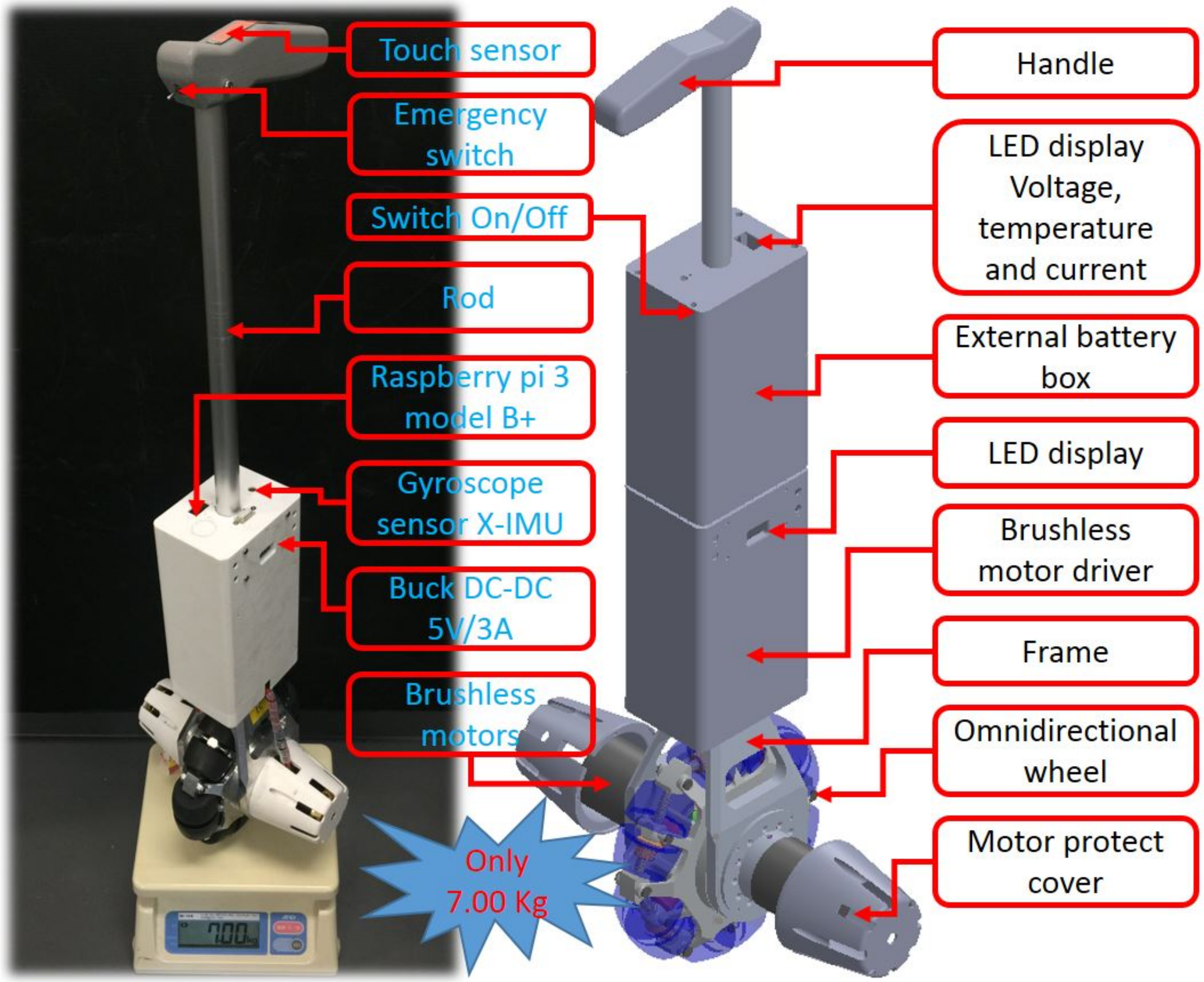

Figure 2.1: Hardware design of the robotic cane.

Another part is a step-down module to convert the power supply voltage from the batteries of 25.2 VDC to 5 VDC of the 3A maximum output. That voltage supplies to the center controller, the mainboard, and the gyroscope sensor. The balance velocity which manages the upright position of the robotic cane is figured out from the velocity and direction of the motorized omnidirectional wheel which is based on the behaviors of the users related to the angle and speed of the rod of the robotic cane.

The balance velocity is figured out from the velocity and direction of the motorized omnidirectional wheel, which requires the robotic cane to be in a substantially upright position. Based on the control signals received from the controller, the controller of the robotic cane either keeps stability around the equilibrium value or aids the user to balance.

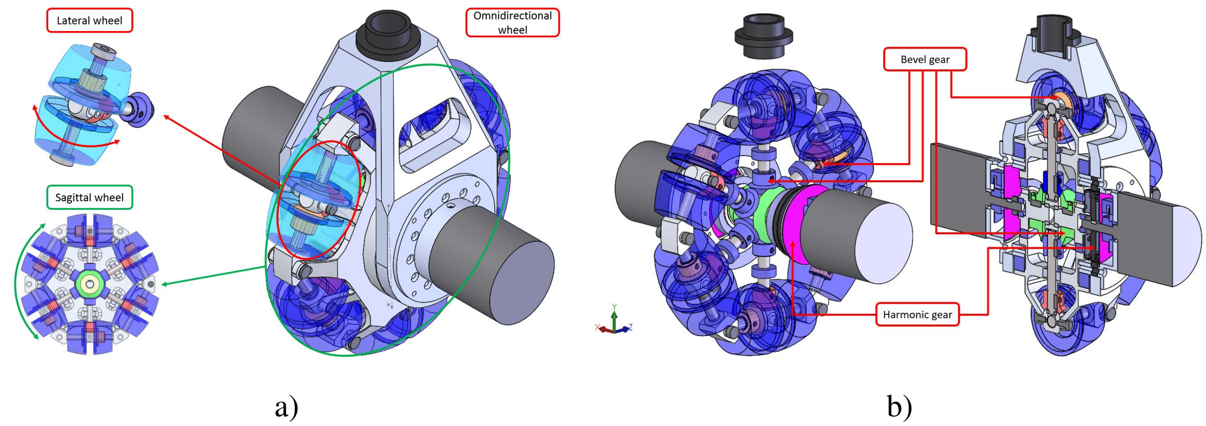

Figure 2.2: Omnidirectional wheel structure including lateral and sagittal wheels (a), Gearbox of the omnidirectional wheel containing bevel gears and harmonic gears (b).

Fig. 2.2 (b) illustrates the internal structure of the gearbox which consists of bevel gears and a harmonic gearbox.

Table 2.1: Harmonic gear factors(CSD-20-50-2A-GR-SP)

Definition	Value	Unit
Reduction ratio	50	
Allowable peak torque of the start and stop time	39	Nm
Maximum allowable momentary torque	69	Nm
Maximum allowable input rotational speed	6500	rpm

More detail information of the harmonic gear is given in Tab. 2.1. The harmonic gear is a special structure gearbox, compact and lightweight. It also has a high torque capability output.

Table 2.2: Motor driver factors (Elmo motion control G-DCWHI20/100EE)

Definition	Value	Unit
Maximum DC supply voltage	95	V
Maximum continuous power output	1600	W
Amplitude sinusoidal/DC continuous current	20	A

The angle of the rod ϕ of the robotic cane is caught by the gyroscope sensor module including an accelerometer. The Scorpion brushless motors are managed by two Elmo motor drivers (Tab. 2.2) standing on motion control technique inside.

Table 2.3: Brushless motor factors(HK-4525-520KV)

Definition	Value	Unit
Stator diameter	45	mm
Stator thickness	25	mm
Shaft diameter	5.98	mm
Weight	470	gram
Max continuous Current	100	A
Max continuous Power	4450	W

The positions of the robotic cane are administered by two Scorpion brushless motors with high torque output driven by two Elmo motor drivers, and absolute encoders. The velocity and the torque of the motors (Tab. 2.3) can control by analog signals corresponding to the current control of the Elmo motor driver.

Table 2.4: Gyroscope sensor module(X-IMU) factors

Definition	Value	Unit
Power supply voltage	3.3 to 6.3	V
Dimensions	33x42x10	mm
Weight	12	gram
Gyroscope range	±2000	degree/s
Accelerometer range	±8	g

These motor drivers are administered by the motion signals getting from the central controller. The control signals depend on the programming algorithms. The complete hardware of the robotic cane includes the batteries. It weighs 7.0 Kg (Fig. 2.1). In order to last the working time of the robotic cane for more than one hour, the external battery is used with a mass of 2.3 kg, voltage of 25.2V, and current of 13.8 Ah.

In order to protect the motors and make sure the safety of the user, a plastic cover, grip handle, and another parts is made by a 3D printer.

The angle and the speed of the rod of the robotic cane are calculated by an X-IMU gyroscope sensor module (Tab. 2.4). A USB interface is usde to connect the central controller to the X-IMU gyroscope sensor module to get the angle and the speed of the rod of the robotic cane. This module included the filter program to remove the noise of the environments, it is very important to control stable of any system, and is also useful to apply to control our system stable.

The angle and velocity of the motors of the robotic cane are calculated by an absolute encoder mounted on the motor shaft. An Inter-Integrated Circuit (I2C) interface is linked to the ADC circuit to control the motions of the motor driver by analog input signals.

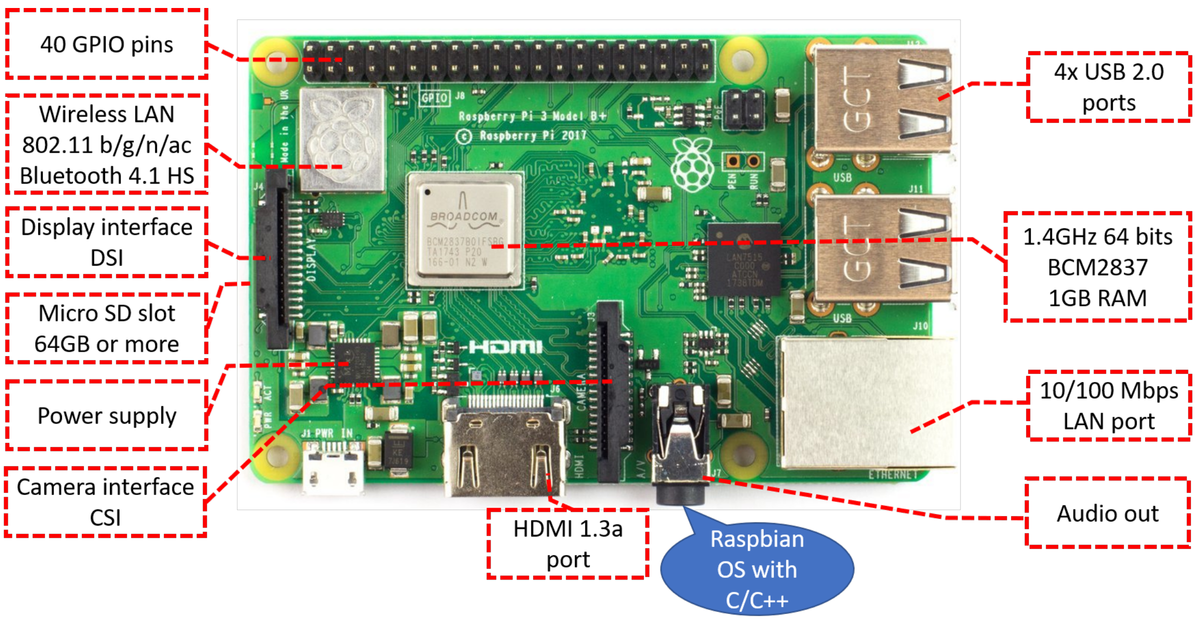

Figure 2.3: Raspberry Pi Model B+ specifications.

A Raspberry Pi 3 Model B+ works as a center controller with high processing and 2GB of the RAM and 16GB of the SD card memory, that is enough to develop our projects. The central controller is a Raspberry Pi 3 Model B+ (Fig 2.3) with a serial peripheral interface associated to a digital-to-analog converter circuit (Fig 2.7 (a)).

The ratchet structure as shown in Fig. 2.4 makes the robotic rotate and keep the robot's state at any position. This guarantees strongly and immediately support by the robotic cane for th user.

A gear key and a latching switch help the ratchet structure turn in only one way. The latch-switch status decides the angular direction. The ratchet structure is quickly stretched out by taking out a spiral spring when the user activates the brake fork. This structure can keep the status of the frame at the present state better other structures.

In some cases, the controller of the system error or the battery has problems, then this emergency safety structure can immediate open to support the user to be strong stable without any problems of falling down or unbalancing.

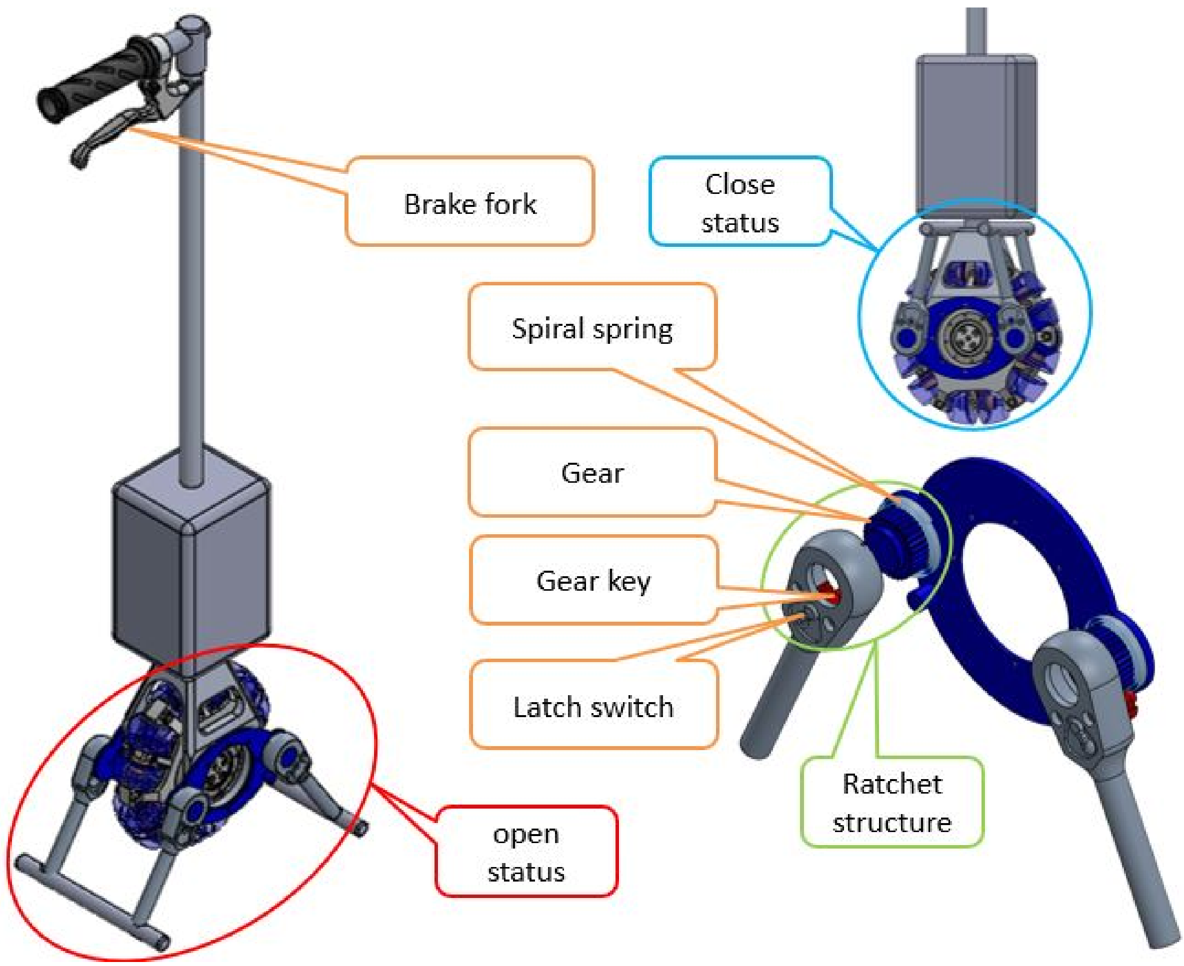

Figure 2.4: Ratchet frame structure for mechanic safety mode.

When the user intends to fall backward or forward, the brake fork on the grip handle immediately stretches out the ratchet structure, and the closed state (Fig. 2.5 (a)) switches to the open state to support the user to be strong stable (Fig. 2.5 (b)).

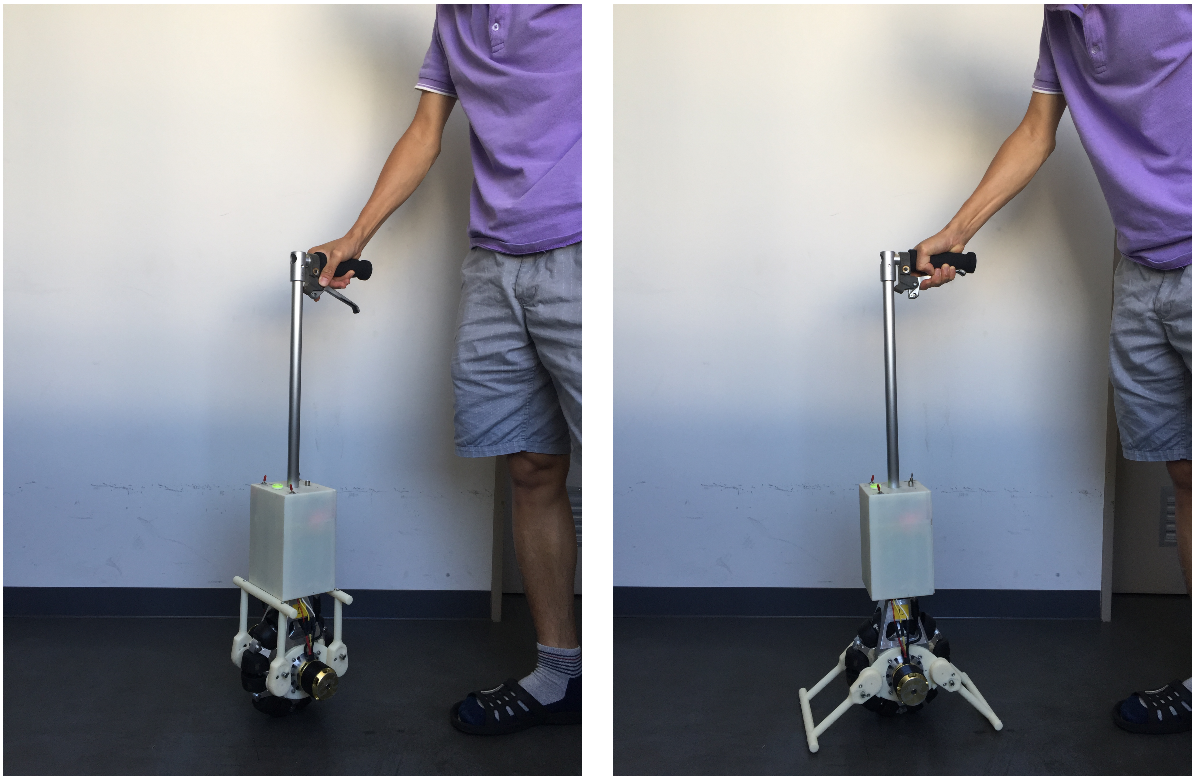

a) b)

Figure 2.5: Ratchet frame status while a robotic cane helps the user to walk: (a) Before open; (b) After open.

2.3 Hardware of the Two-wheeled Cane

The hardware of the two-wheeled cane which uses a natural rubber tire in-wheel electric motor is discussed in this part.

As shown in Fig. 2.6 (a), the two-wheeled cane includes a grip handle mounted on the top of the robot which is connected to the frame of the cane by an aluminum rod. This frame was made by utilizing a computer numerical control (CNC) machine. It is linked to two natural rubber tire electric wheels (Fig. 2.6 (c)) on the left and right sides to manage the motions of the two-wheeled cane.

Two Maxon motor drivers are used on the left and right sides of the body to adjust the output current of 10 A to the natural rubber tire electric wheels including a brushless motor. At the middle of the body, Li-ion batteries with a protection circuit board are installed (Fig. 2.7 (b)) with a capacity of 36 V/4400 mAh and maximum power is 42 V in full charge to ensure that the two-wheeled cane can work continuously in more than 10 hours without charging.

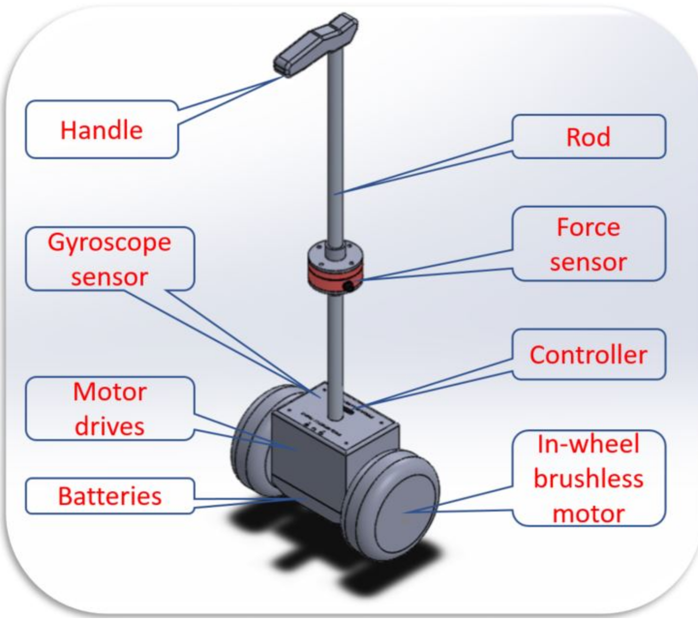

a)

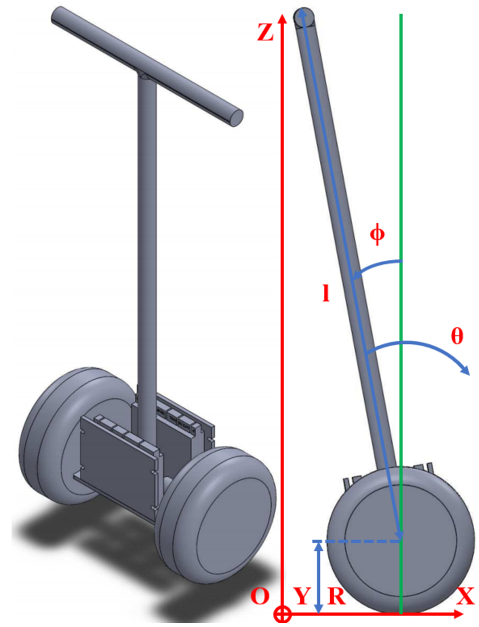

b)

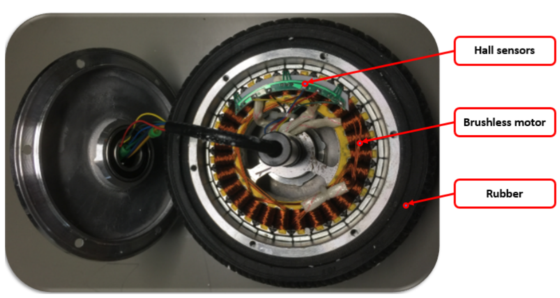

c)

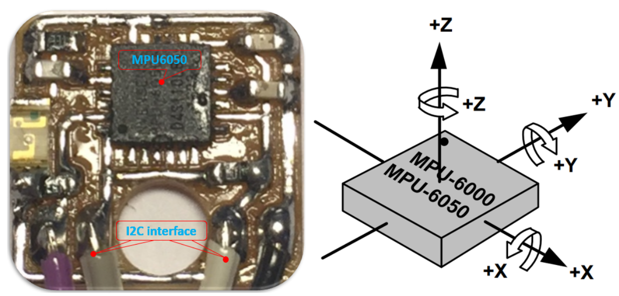

d)

Figure 2.6: Hardware design of the two-wheeled cane (a), Coordinate system of the two-wheeled cane (b), In-wheel motor (c), MPU6050 circuit board (d).

As shown in Fig. 2.6 (c), to control the movements of the robot, the natural rubber tire electric wheel is used. It includes a brushless motor and Hall sensors. The two-wheeled cane can work well in any environments. More detail information of the structure is provided in Tab. 2.5.

By using only this special of in-wheel motor not including any gearbox types, the two-wheeled cane can operate smoothly without any noises and turn with a small power connection, this is impossible with other motor-included gear types.

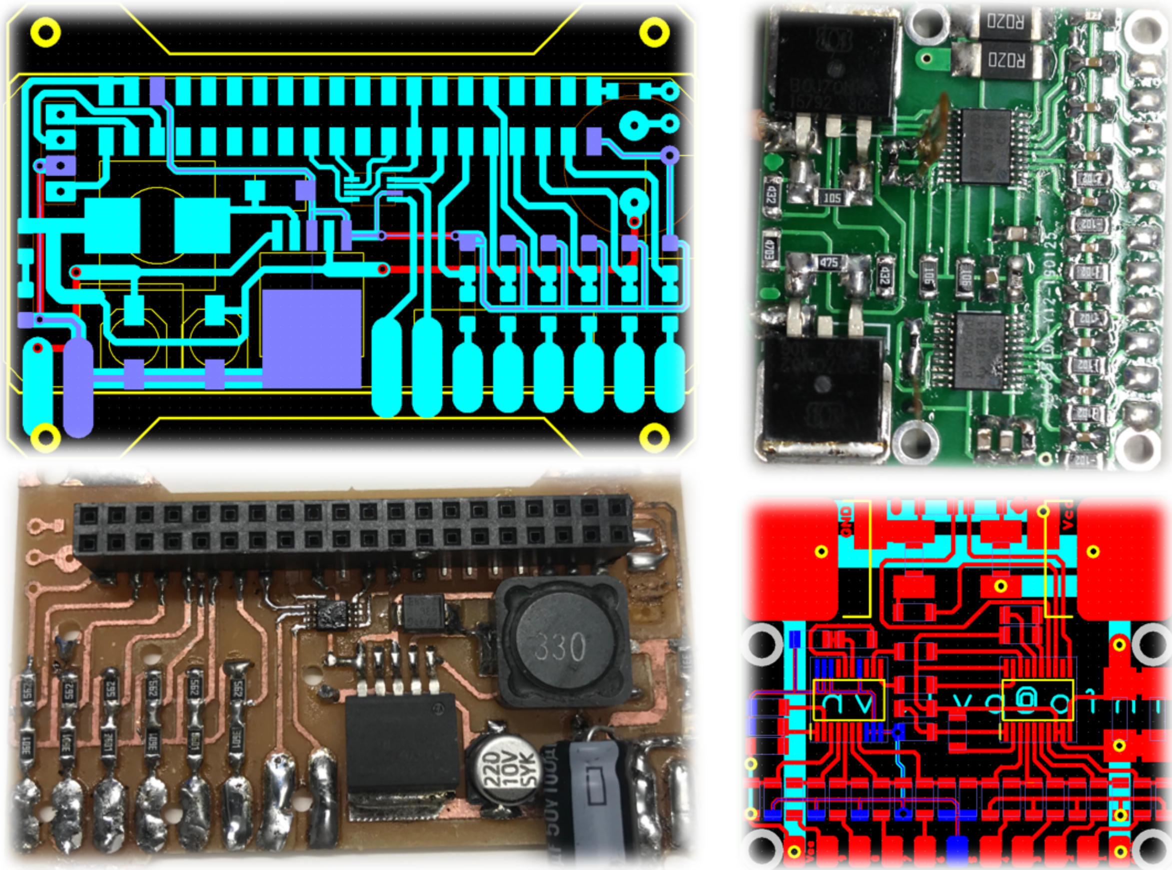

a) b)

Figure 2.7: Designed circuit: Bridge circuit board (a) and battery circuit protection board (b).

In addition, as shown in (Fig. 2.6 (d)) the MPU6050 accelerometer and gyroscope sensor are cheap devices, easy to buy. The MPU6050 chips are connected to a 3-axis gyroscope with a changeable range up to ±2000 degree/s, and a 3-axis accelerometer with a changeable range up to ±8 g and 400 kHz and a fast mode I^2C to make communication with all registers to simply associate to the center controller.

A center controller installed at the bottom is a Raspberry Pi Zero W controller with 1GB RAM, 16GB SD card memory, and a bridge circuit board (Fig. 2.7 (a)) connected to an accelerometer and a gyroscope sensor by using I2C interface to figure out and control the movements of the two-wheeled cane following the control algorithm.

Moreover, one SPI interface is used in the bridge board to connect between the central controller and the analog signal to control the motions of the motors through the Maxon motor driver input signal pins.

Table 2.5: The natural rubber tire electric wheel factors

Definition	***Symbol***	***Unit***	***Values***
Voltage	V	V	36
Output power	P	W	250
Hall sensor	H	PPR	90
Size (thickness x diameter nominal)	S	mm	46 x 168

Moreover, to control the motions of the brushless motor through the maxon motor driver by current control, the analog input pin of the driver control is used by a digital to analog converter board using SPI interface to connect to the center controller.

2.4 Hardware of a Two-wheeled Walker

In this section, a new type of assistance robot is introduced. It consists of a special U-shaped frame to support the full bodyweight of the user to walk or stand.

Firstly, as shown in Fig. 2.8, the hardware of the two-wheeled walker is simulated by the Solidworks software, and then it is manufactured by our university workshop.

Thanks to a U-shaped special frame, the user can hold to be supported or ride on it. Two wheels with an in-wheel motor include brushless motor, hall sensors, a natural rubber tire with air, a battery pack, a controller, a gyroscope sensor MPU6050, and two Maxon motor drivers as shown in Fig. 2.9.

Stainless steel pipe material is used with a thickness of 2 mm. Thus, the U-shaped structure can support the user to stand or to walk with his whole bodyweight. The key holders on both sides of the frame are equipped. Besides, the height of the robot can be easily adjusted following on the height of the user.

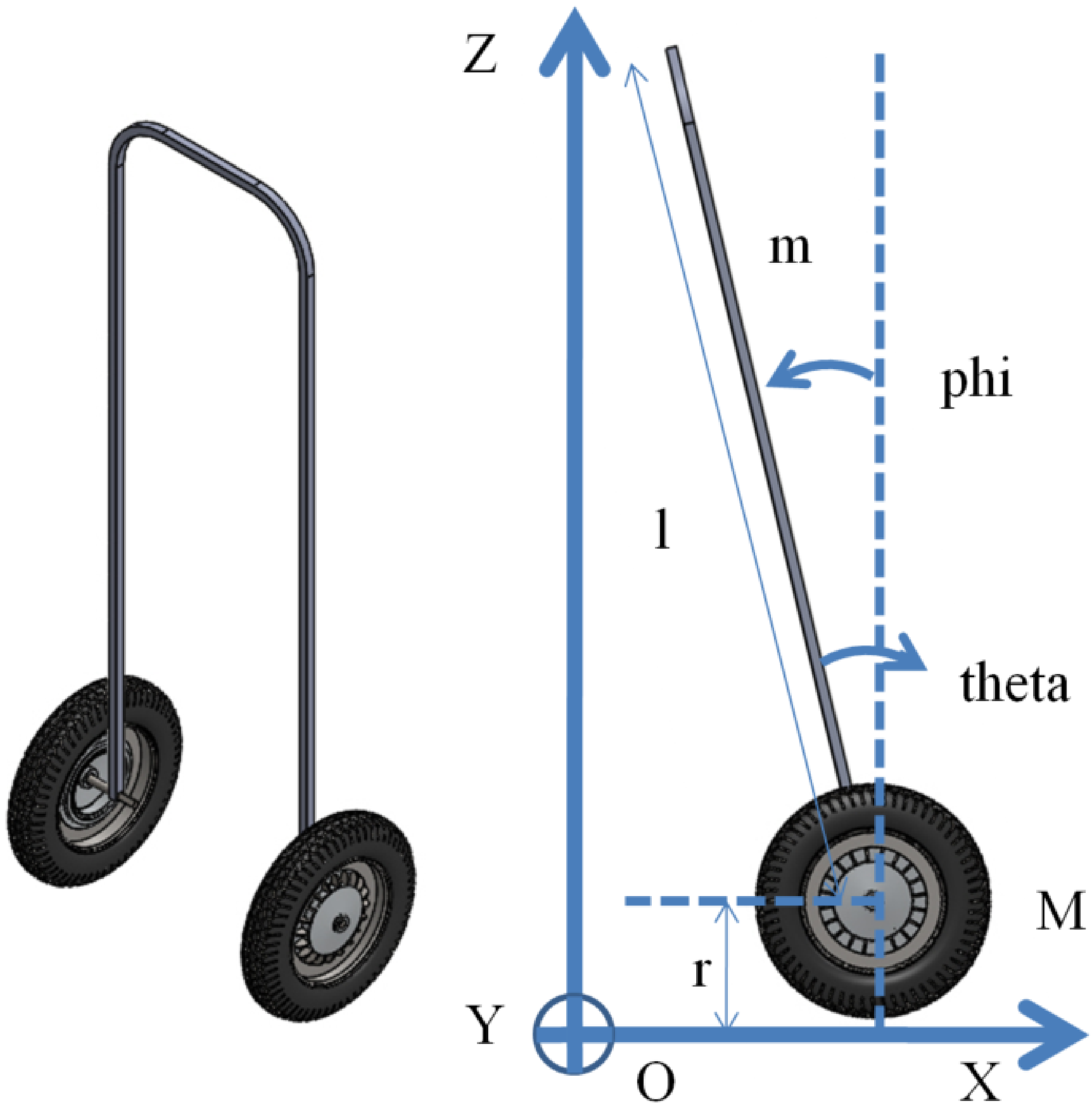

Figure 2.8: Design of the two-wheeled walker.

The natural rubber tire with airflow creates strong torques and makes the user feel comfortable due to the elimination of vibrations. The in-wheel electric motor works as a motor. Besides, it contains three hall sensors which figure the rotation movements of the motor and the velocity of the two-wheeled walker.

It is shown in Fig. 2.9 (b) that the battery pack contains 10 cells of 3.7 V/3200 mAh lithium-ion batteries in series to create a maximum power supply of 42 V when it was entirely energized.

Thus, the two-wheeled walker can work in more than 10 hours without charging. A step-down circuit board is added to create a 5V/3A output to supply the controller. This board utilizes a LM2597HV IC which is directly supplied by a high voltage input from this battery pack of 42V. The 5 V/3 A output suits the Raspberry Pi 3 Model B+ which works as the controller.

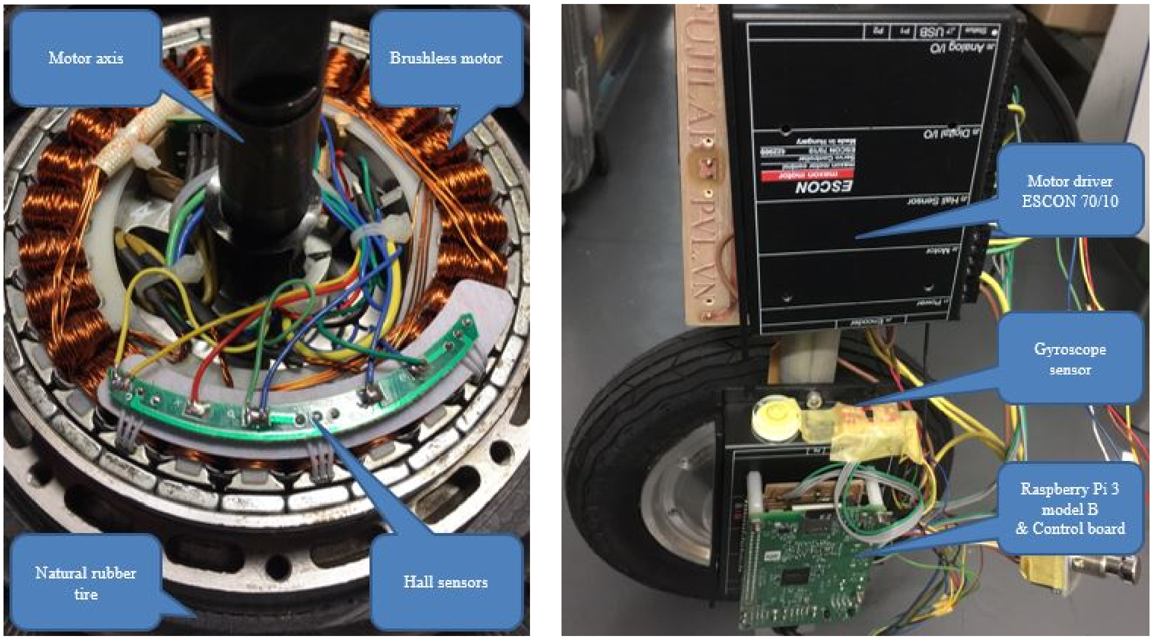

a) b)

Figure 2.9: In-wheel motor (a), Maxon motor driver (ESCON 70/10) (b).

The center controller is a Raspberry Pi 3 Model B+ built on the Raspbian OS for C/C++ coding. It controls the system in the real-time with 2GB RAM and 16GB SD card memory which is big enough for our study.

Two Maxon motor drivers (ESCON 70/10) are utilized to control the movements of the two-wheeled walker by the current control approach. These motor drivers can manage the current of the motor from -10A to 10A based on the analog signal input pins. However, we keep it at 5A to ensure the two-wheeled walker to be safe for the user and itself in experiments.

The gyroscope sensor module with MPU6050 IC (Fig. 2.6 (d)) is installed to figure out the angle and the speed of the rod of the two-wheeled walker, these are important values to control the movements of the two-wheeled walker.

2.5 Summary

This chapter presents the complete hardware design of the robotic canes for walking assistance built on an inverted pendulum model. The hardware design plays a very important role for any assistance devices. Whether the control algorithm can be applied to the system successfully or not depends on whether the hardware design is well designed or not. Moreover, in order to support the user to maintain balance in practice, the hardware design of the robotic canes should be considered carefully in term of safety. In our design, we add the safety structure to protect the user, and develop the robotic cane with a complete design and the high speed controller based on Raspberry Pi Model B+ as a center controller.

The ratchet mechanic structure, the battery and the sensors are included on the body of the system for the safety. The two-wheeled cane and the two-wheeled walker for walking assistance also have fabricated by utilizing the in-wheel motor with fast response to the user's behavior and safe power. All of the robotic canes have designed completely after considering carefully issues like safety and the working time of battery.

Chapter 3

Mathematical Model and the Design of Controller of the Robotic Canes

3.1 Abstract

A basic inverted pendulum model of a traditional mechanical system is developed on this study. In previous researchers, the stability of the inverted pendulum model was controlled by variety of different methods: basic control loop feedback [23]; fuzzy-logic controller [1, 18]; a linear quadratic regulator (LQR) [13, 14]; additional sliding-mode control (SMC) [2, 6]; newton networks [21, 24], and a new NDOB [7]. The authors [10, 19] have controlled the position and the velocity of a popular inverted pendulum model by two new controllers. These installed controllers ensure a strong and stable position of the robot at the desired simulation point, but the performance of these controllers are not verified in real experiments. The authors in [3] have also controlled the torque and the velocity of an inverted pendulum motor in an analytical simulation study, and describe equal exchange between control methods in different application cases.

All of the previous studies have focused on the stability of the inverted pendulum only around the equilibrium point or around zero degree. However, these values are too small and unsuitable for walking assistance robot as our robotic canes. To support the user stable and to walk, all

walking assistance robots need to strong stable far from the zero position. This thesis resolves the equilibrium issue through the LAM and the NDOB with the balancing point not only around zero degrees as the above-mentioned popular methods. The LAM is simply applied to the nonlinear controller and linearizes of the nonlinear system of the robotic canes even when the balancing angle largely differs from equilibrium points whereas the NDOB estimated the user's external force is also applied to the robotic canes to control the motions of the robotic canes following the user's behaviors. Therefore, the robotic canes are provided with a fall prevention functionality which is a highly desirable point of any walking assistance device. The user may not be fallen forward or backward when he uses the robotic canes to walk or to stand.

The author in [29] has presented in detail about the NDOB and achieved the simulation results of a mono-wheel robot model.

The studies in [25–28] and [29] stopped in the form of simulation models, have shown that to apply these studies to practical applications, they need to be researched and developed more. When applying the LAM and NDOB into our robotic canes on the application model, we developed it in the form of adding an intelligent mode switch to the central controller to be able to meet the practical application of the robotic canes for walking assistance.

This chapter presents a mathematical model of the robotic canes built on the inverted pendulum model. This method is calculated by using Lagrangian motion equations to find the equations of the motion of the robotic canes as a nonlinear system. To linearize this nonlinear system, the LAM used by the authors in [25–28] will be reminded in this section with serial simulation results on the robotic cane by adding some functions to the controller such as a low-pass filter. Moreover, the NDOB proposed in [29] is also represented and applied to our controller to find the external human force put on the robotic cane to control the motion of the system following the user behaviors. The combination between the LAM with the NDOB as well as smart mode switching can control the motions of the robotic cane more convenient as well as effective for the user.

3.2 Mathematical Model of the Robotic Canes

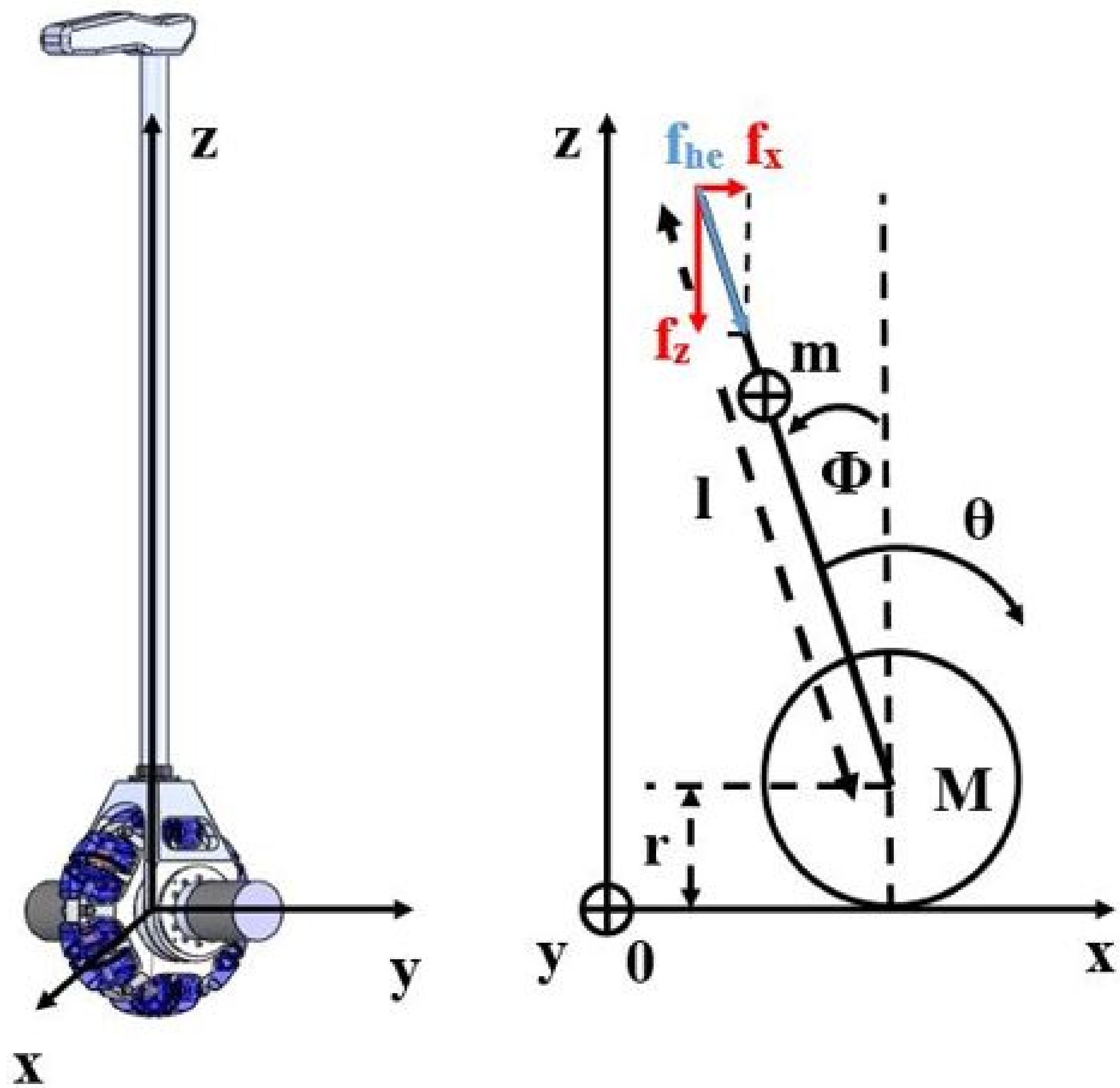

Figure 3.1: The standard coordinate system of the robotic cane.

By using the specially designed gear box (mentioned in the previous chapter), the rotation angles of the omnidirectional wheel are associated to the rotation angles of the two motors as given in (3.1) and (3.2):

$$\theta_{Pitch} = G_H \frac{\theta_R + \theta_L}{2} \tag{3.1}$$

$$\theta_{Roll} = G_B G_H \frac{\theta_R - \theta_L}{2} \tag{3.2}$$

where θ_{Pitch}, θ_{Roll}, θ_R, and θ_L express the angles of the major wheel, the minor wheel, the left motor and the right motor, correspondingly while G_H and G_B are the gear reduction ratios of the harmonic and bevel gears correspondingly, with $G_H = 1/50$ (Tab. 2.1) and $G_B = 2$.

From (3.1) and (3.2), the wheel torques that administer the inverted pendulum in the sagittal and lateral planes are delivered to the motor torques and the controller are seamlessly administered by Eqs. (3.3) and (3.4).

$$\tau_R = \frac{1}{G_H}\tau_{Pitch} + \frac{1}{G_B G_H}\tau_{Roll} \tag{3.3}$$

$$\tau_L = \frac{1}{G_H}\tau_{Pitch} - \frac{1}{G_B G_H}\tau_{Roll} \tag{3.4}$$

Fig. 3.1 illustrates the standard coordinate system. The system consists of two primary planes: a sagittal plane $(x - z)$, and a lateral plane $(y - z)$. In these planes, the robotic cane is considered as an inverted pendulum with one large wheel and small wheels, correspondingly.

The torques are applied on the left and right motors figured out by (3.1) and (3.2), correspondingly. They are identical both the sagittal and the lateral planes, but they are different in their input parameters.

The mathematical symbols in formulas are described as in Tab. 3.2, and the motion equations are given by:

$$\frac{d}{dt}\left(\frac{\partial L}{\partial \dot{\phi}}\right) - \frac{\partial L}{\partial \phi} + \frac{\partial F_{fr}}{\partial \dot{\phi}} = 0 - d_1 \tag{3.5}$$

$$\frac{d}{dt}\left(\frac{\partial L}{\partial \dot{\theta}}\right) - \frac{\partial L}{\partial \theta} + \frac{\partial F_{fr}}{\partial \dot{\theta}} = \tau - d_2 \tag{3.6}$$

where L is the Lagrangian and the other parameters are details in (3.7)-(3.14):

$$L = T - V \tag{3.7}$$

$$F_{fr} = \frac{1}{2}D_\phi\dot{\phi}^2 + \frac{1}{2}D_\theta\dot{\theta}^2 \tag{3.8}$$

$$T_1 = \frac{1}{2}J_\theta(\dot{\theta} - \dot{\phi})^2 \tag{3.9}$$

$$T_2 = \frac{1}{2}J_\phi\dot{\phi}^2 \tag{3.10}$$

$$T_3 = \frac{1}{2}Mr^2(\dot{\theta} - \dot{\phi})^2 \tag{3.11}$$

$$T_4 = \frac{1}{2}m([\frac{d}{dt}(r(\theta - \phi) - l\sin\phi)]^2 + [\frac{d}{dt}(l\cos\phi)]^2) \tag{3.12}$$

$$T = \sum_{i=1}^{4} T_i \tag{3.13}$$

$$V = mgl\cos\phi \tag{3.14}$$

The transmission function matrix of the inverted pendulum model to clarify the robotic cane's motions can be recapped as follows:

$$\begin{bmatrix} H_{11} & H_{12} \\ H_{21} & H_{22} \end{bmatrix}\begin{bmatrix} \ddot{\phi} \\ \ddot{\theta} \end{bmatrix} + \begin{bmatrix} b_1 \\ b_2 \end{bmatrix} = \begin{bmatrix} -d_1 \\ \tau - d_2 \end{bmatrix} \tag{3.15}$$

The parameters of this equation are given by (3.16)-(3.20):

$$H_{11} = J_\theta + (M + m)r^2 + 2mrl\cos\phi + J_\phi + ml^2 \tag{3.16}$$

$$H_{12} = H_{21} = -J_\theta - (M + m)r^2 - mrl\cos\phi \tag{3.17}$$

$$H_{22} = J_\theta + (M + m)r^2 \tag{3.18}$$

$$b_1 = -\dot{\phi}^2 mrl\sin\phi - mgl\sin\phi + D_\phi\dot{\phi} \tag{3.19}$$

$$b_2 = \dot{\phi}^2 mrl\sin\phi + D_\theta\dot{\theta} \tag{3.20}$$

To control the motions of the robotic cane we need to applied the torque on the motor axis on the left and the right sides of the gear box, which is calculate by:

$$\tau = (H_{22} - \frac{H_{12}H_{21}}{H_{11}})u - \frac{H_{21}}{H_{11}}b_1 - \frac{H_{21}}{H_{11}}d_1 + b_2 + d_2 \tag{3.21}$$

3.3 Linearization of the Nonlinear System by Using LAM

When the form of (3.22) is recast, the motion equations of (3.15) of the robotic cane are easily determined as a nonlinear system.

$$\dot{x} = \begin{bmatrix} \dot{\phi} \\ \ddot{\phi} \\ \dot{\theta} \\ \ddot{\theta} \end{bmatrix} = \begin{bmatrix} \dot{\phi} \\ -\frac{b_1}{H_{11}} - \frac{d_1}{H_{11}} \\ \dot{\theta} \\ 0 \end{bmatrix} + \begin{bmatrix} 0 \\ -\frac{H_{12}}{H_{11}} \\ 0 \\ 1 \end{bmatrix} u \tag{3.22}$$

The LAM expression is utilized to linearize the nonlinear system as shown below:

$$\dot{x} = f(x) + g(x)u \tag{3.23}$$

$$y = h(x) \tag{3.24}$$

The input value u define by:

$$u = \alpha(x) + \beta(x)v \tag{3.25}$$

where v expresses the external reference input.

$$L_f h(x) = \sum_{i=1}^{n} \frac{\partial h}{\partial x_i} f_i(x) = \frac{\partial h}{\partial x}(x) f(x) \tag{3.26}$$

The derivative of y by t is in detail as below:

$$\frac{dy}{dt} = \frac{\partial h}{\partial x}\frac{\partial x}{dt} = \frac{\partial h}{\partial x}(f(x) + g(x)u) = L_f h(x) + L_g h(x)u \tag{3.27}$$

Linking this equation to the below law (3.28) [8], with $r < n$:

$$\begin{cases} L_g {L_f}^{(r-1)} h \neq 0 \\ L_g h = L_g L_f h = L_g {L_f}^2 h = ... = L_g {L_f}^{(r-2)} h = 0 \end{cases} \tag{3.28}$$

By using this rules, the extended equations of y by t can determine as written in (3.29)-(3.31):

$$\dot{y} = L_f h \tag{3.29}$$

$$\ddot{y} = {L_f}^2 h \tag{3.30}$$

$$\vdots$$

$$y^{(r)} = {L_f}^r h(x) + L_g {L_f}^{(r-1)} h(x) u \tag{3.31}$$

where the input value of u of the controller is taken account by the closed loop system with $y^{(r)} = v$:

$$u = \frac{v - {L_f}^r h(x)}{L_g {L_f}^{(r-1)} h(x)} \tag{3.32}$$

We declare y as a function of ϕ and θ in (3.33). Thus, the derivatives of y with respect to t are determined by (3.34) and (3.35) as below.

$$y = \sigma_1(\phi) + \sigma_2(\theta) \tag{3.33}$$

$$\dot{y} = \frac{\partial \sigma_1(\phi)}{\partial \phi}\dot{\phi} + \frac{\partial \sigma_2(\theta)}{\partial \theta}\dot{\theta} \tag{3.34}$$

$$\begin{aligned} \ddot{y} =& \frac{\partial^2 \sigma_1(\phi)}{\partial \phi^2}\dot{\phi}^2 + \frac{\partial^2 \sigma_2(\theta)}{\partial \theta^2}\dot{\theta}^2 - \frac{b1}{H_{11}}\frac{\partial \sigma_1(\phi)}{\partial \phi} \\ &- \left(\frac{H_{12}}{H_{11}}\frac{\partial \sigma_1(\phi)}{\partial \phi} - \frac{\partial \sigma_2(\theta)}{\partial \theta}\right)u \end{aligned} \tag{3.35}$$

Comparing (3.35) with the law in (3.28), we have:

$$\frac{H_{12}}{H_{11}}\frac{\partial \sigma_1(\phi)}{\partial \phi} - \frac{\partial \sigma_2(\theta)}{\partial \theta} = 0 \tag{3.36}$$

From (3.36), the elements of (3.33) can be found as follows:

$$\frac{\partial \sigma_1(\phi)}{\partial \phi} = \frac{H_{11}}{H_{12}} \tag{3.37}$$

$$\frac{\partial \sigma_2(\theta)}{\partial \theta} = 1 \tag{3.38}$$

Thus, (3.33) is redefined as follows:

$$y = \int_0^{\phi} \frac{H_{11}}{H_{12}} d\phi + \theta \tag{3.39}$$

As the same way, the derivatives of the new variable of y are figured by (3.40)-(3.43). These equations express the linearized equations of the nonlinear system of the robotic cane:

$$y = \int_0^{\phi} \frac{H_{11}}{H_{12}} d\phi + \theta \tag{3.40}$$

$$\dot{y} = \frac{H_{11}}{H_{12}}\dot{\phi} + \dot{\theta} \tag{3.41}$$

$$\ddot{y} = \frac{\partial}{\partial \phi}\frac{H_{11}}{H_{12}}\dot{\phi}^2 - \frac{b_1}{H_{12}} \tag{3.42}$$

$$y^{(3)} \simeq \frac{\partial^2}{\partial \phi^2}\frac{H_{11}}{H_{12}}\dot{\phi}^3 - \frac{\partial}{\partial \phi}\frac{b_1}{H_{12}}\dot{\phi} - 2\left(\frac{\partial}{\partial \phi}\frac{H_{11}}{H_{12}}\right)\frac{b_1}{H_{11}}\dot{\phi} \tag{3.43}$$

The expansion (3.32) is applied with the derivative rank $r = 4$ by simplifying the analysis and programming based on the center controller processing. The input value u in 3.32 should be changed as below:

$$u = \frac{v - {L_f}^4 h(x)}{L_g {L_f}^3 h(x)} \tag{3.44}$$

The parameters in (3.32) are similar to those in (3.45)-(3.46):

$$\begin{aligned} L_g {L_f}^3 h(x) = &- 3\frac{\partial^2}{\partial\phi^2}\frac{H_{11}}{H_{12}}\frac{H_{12}}{H_{11}}\dot{\phi}^2 + \frac{\partial}{\partial\phi}\frac{b_1}{H_{12}}\frac{H_{12}}{H_{11}} \\ &+ 2\frac{\partial}{\partial\phi}\frac{H_{11}}{H_{12}}\frac{H_{12}}{{H_{11}}^2}b_1 \end{aligned} \tag{3.45}$$

$$\begin{aligned} {L_f}^4 h(x) = &- \frac{\partial^2}{\partial\phi^2}\frac{b_1}{H_{12}}\dot{\phi}^2 + \frac{\partial^3}{\partial\phi^3}\frac{H_{11}}{H_{12}}\dot{\phi}^4 \\ &- 5(\frac{\partial^2}{\partial\phi^2}\frac{H_{11}}{H_{12}})\frac{b_1}{H_{11}}\dot{\phi}^2 - 2\frac{\partial}{\partial\phi}\frac{H_{11}}{H_{12}}\frac{\partial}{\partial\phi}\frac{b_1}{H_{11}}\dot{\phi}^2 \\ &+ \frac{\partial}{\partial\phi}\frac{b_1}{H_{12}}\frac{b_1}{H_{11}} + 2\frac{\partial}{\partial\phi}\frac{H_{11}}{H_{12}}\left(\frac{b_1}{H_{11}}\right)^2 \end{aligned} \tag{3.46}$$

Therefore, the controller coefficient is declared as:

$$v = -\sum_{i=0}^{3} \lambda_i (y^{(i)} - y_{ref}^{(i)}) \tag{3.47}$$

From here, many of the methods can be learned to find these factors such as the pole placement method.

3.4 Nonlinear Disturbance Observer

The common motion equation of the inverted pendulum model is recast as follows:

$$\frac{\mathrm{d}}{\mathrm{dt}}\left(\frac{\partial \mathrm{L}}{\partial \dot{q}}\right) - \frac{\partial \mathrm{L}}{\partial q} = \tau_{all} - d \tag{3.48}$$

where d is the generalized external torque put by the user on the top of the rod.

The state space of the NDOB [27] is represented by

$$\dot{\xi} = -K\xi + K^2\frac{\partial L}{\partial \dot{q}} + K(\frac{\partial L}{\partial q} + \tau_{all}) \tag{3.49}$$

$$\hat{d} = \xi - K\frac{\partial L}{\partial \dot{q}} \tag{3.50}$$

where $\hat{d}$ denotes the estimated disturbance, ξ expresses the observer state variables, L means the Lagrangian, and K shows the gain of the observer.

The human external force f_{he} in the coordinate system of Fig. 3.1 is separated into a vertical component f_z and a horizontal component f_x (or f_y). These two forces are denoted as d_1 and d_2, correspondingly, are figured by

$$d_1 = (-l_c \cos\phi - r) f_x - l_c \sin\phi f_z \tag{3.51}$$

$$d_2 = r f_x circumvolution \tag{3.52}$$

The external forces put on the robotic cane by the user during the motion of the robotic cane with the user, are not computed by human force sensors. The translational (x-or y-directional) motion of the cane is similar to the axial circumvolution of the robotic cane, while the vertical (z-direction) corresponds to the motion of its rod. The external force put by the user is caught from the NDOB as follows (Fig. 3.3):

$$\hat{f}_x = \frac{\hat{d}_2}{r} \tag{3.53}$$

$$\hat{f}_z = -\frac{1}{l_c r \sin\phi} \left\{ (l_c \cos\phi + r)\hat{d}_2 + r\hat{d}_1 \right\} \tag{3.54}$$

The angle reference of the rod ϕ_{ref} is computed from the disturbance force $\hat{d}_1$ as:

$$\phi_{ref} = \sin^{-1} \frac{\hat{d}_1}{l_c m g} \tag{3.55}$$

The wheel angle reference, declaring the demanded space to transfer from the current angle rod $\phi_{current}$ to the reference rod angle, is figured as follows:

$$\theta_{ref} = \frac{l_c \sin\phi_{ref}}{r} \tag{3.56}$$

The wheel angular velocity has proportion to the integral of the human force put on the rod of the robotic cane d_2, the external torque that makes the wheel rotate.

$$\dot{\theta}_{ref} = K_I \int \frac{\hat{d}_2}{r} dt \tag{3.57}$$

where K_I is the integral gain.

In terms of the reference factors, the controller equations are reproduced as follows:

$$y_r = \int_0^{\phi_r} \frac{H_{11}}{H_{12}} d\phi_r + \theta_r \tag{3.58}$$

$$\dot{y}_r = \frac{H_{11}}{H_{12}}\dot{\phi}_r + \dot{\theta}_r \tag{3.59}$$

$$\ddot{y}_r = \frac{\partial}{\partial \phi_r}\frac{H_{11}}{H_{12}}\dot{\phi}_r^2 - \frac{b_1}{H_{12}} \tag{3.60}$$

$$y_r{}^{(3)} \simeq \frac{\partial^2}{\partial {\phi_r}^2}\frac{H_{11}}{H_{12}}\dot{\phi}_r^3 - \frac{\partial}{\partial \phi_r}\frac{b_1}{H_{12}}\dot{\phi}_r - 2\left(\frac{\partial}{\partial \phi_r}\frac{H_{11}}{H_{12}}\right)\frac{b_1}{H_{11}}\dot{\phi}_r \tag{3.61}$$

and the coefficients of their equations as given in (3.62) - (3.66):

$$H_{11} = J_\theta + (M+m)\,r^2 + 2mrl\cos\phi_r + J_\phi + ml^2 \tag{3.62}$$

$$H_{12} = H_{21} = -J_\theta - (M+m)\,r^2 - mrl\cos\phi_r \tag{3.63}$$

$$H_{22} = J_\theta + (M+m)\,r^2 \tag{3.64}$$

$$b_1 = -\dot{\phi}_r^2 mrl\sin\phi_r - mgl\sin\phi_r + D_\phi\dot{\phi}_r \tag{3.65}$$

$$b_2 = \dot{\phi}_r^2 mrl\sin\phi_r + D_\theta\dot{\theta}_r \tag{3.66}$$

The torque put to the robotic cane is figured from the measured force F_x along the x-axis and the torque M_y on the y-axis as follows:

$$d = F_x l_x + M_y \tag{3.67}$$

where l_x is the length on the x-axis between the force sensor CFS080CS102A (Tab. 3.1) and the motor axis, and M_y is shown in Fig. 3.2.

For example, the disturbance along the x-axis is contrasted with that evaluated by (3.50) on the x axis.

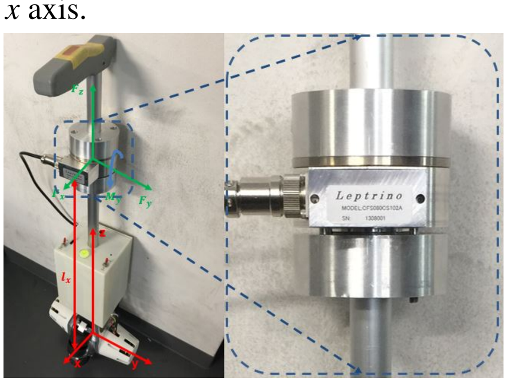

Figure 3.2: Force sensor.

Definition	Value	Unit
Power supply voltage	5	V
Dimensions	80	mm
Rated load Fx,Fy,Fz	1000	N
Rated load Mx,My,Mz	30	Nm
Interface RS422	460800	bps

Table 3.1: Force sensor CFS080CS102A

The results are illustrated in Fig. 3.3. The force calculated by the nonlinear disturbance observer almost matched to the force figured by the force sensor over the whole period, which confirms the proper working ability of the proposed nonlineargovern disturbance observer.

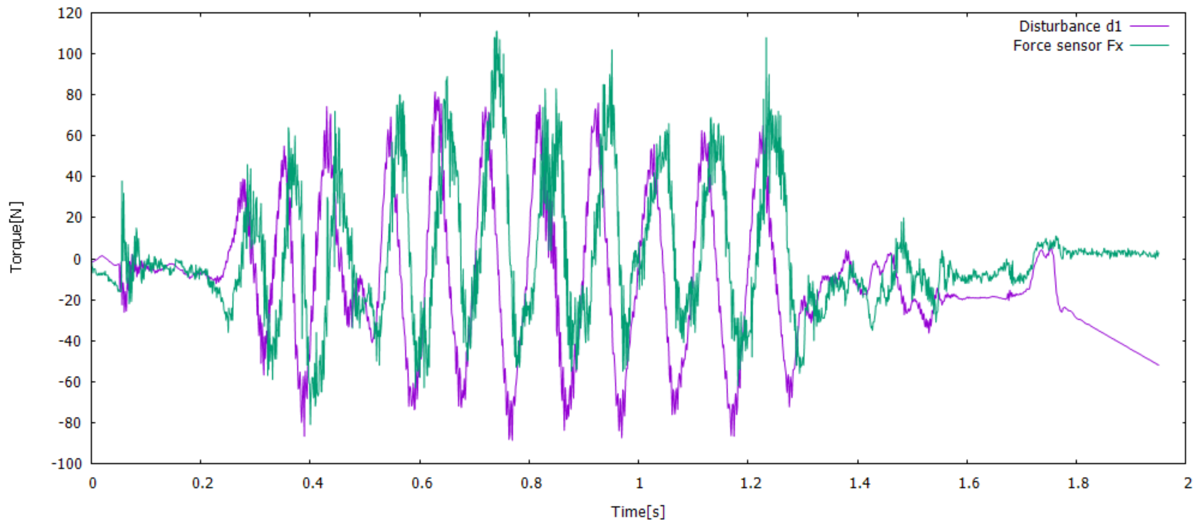

Figure 3.3: Similarity of the estimated torque (purple) and the measured torque (green) by non-linear disturbance observer in the x-axis.

The Root Mean Square Error (RMSE) index is 0.004891. This reveals that the proposed nonlinear disturbance observer is surely similar to the real values getting from the sensor.

From these results, it can be seen that we can totally apply the NDOB to the nonlinear system to determine the external force applied to the systems.

3.5 Controller of the Robotic Cane

Figure 3.4 illustrates the structure of the controller administered by the above-mentioned equations. The coordinate conversion equations decide the current state of the robotic canes. From these coordinate conversion equations, the nonlinear disturbance observer computes the reference signal of the robotic canes.

This structure of the controller can not only applied in the robotic cane, but also work well in the two-wheeled cane and the two-wheeled walker or any inverted pendulum models.

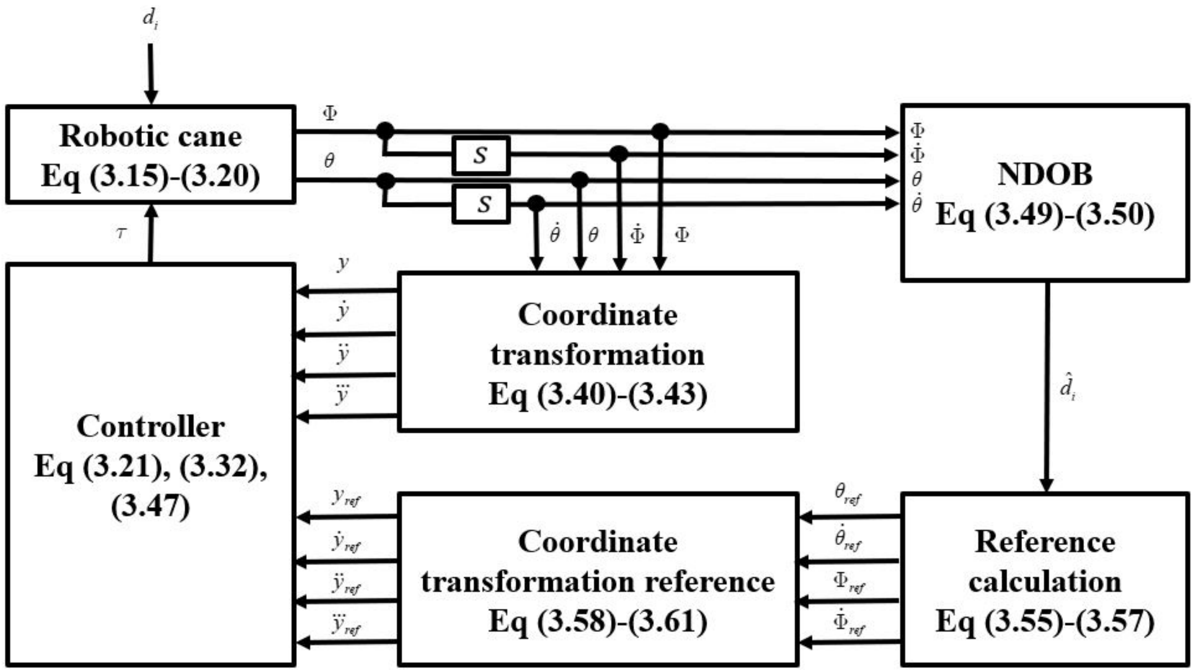

Figure 3.4: Controller of the robotic canes.

3.6 Smart Mode Switching Algorithm

To assist users in the best way, the controller needs to switch flexibly between control modes (balance mode and support mode) to support the user. These modes can be found clearly in Fig. 3.6. Two modes are specified corresponding to the two coefficients of the controller (3.68) corrected by the alpha smoothing factor (3.70). The β shift coefficient is associated with the τ_{ref} shifting position as shown Fig. 3.6.

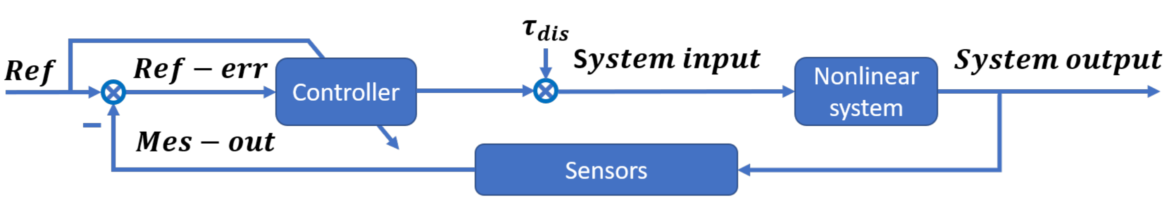

Figure 3.5: Block diagram of the gain scheduling nonlinear system.

As shown in Fig. 3.5, depending on the torque applied to the robotic canes, the controller will smart change to reference input values of the controller to control the system follow the behaviors of the user.

Gain of the nonlinear controller can be calculated by equation:

$$v_k = \sum_{i=0}^{r} \lambda_{ki}(y^{(i)} - y_{ref}^{(i)}) \tag{3.68}$$

and v_{sum} is the total gain can be apply to the controller when change the modes smoothly.

$$v_{sum} = \alpha v_1 + (1 - \alpha)v_2 \tag{3.69}$$

with, v_1 and v_2 is the gain of standing mode and support mode, respectively.

$$\alpha = \frac{|\tau_{dis}|}{|\tau_{dis\,\max}|} \tag{3.70}$$

while τ_{ref}, β, and $\tau_{dis\,\max}$ are determined by our experiments.

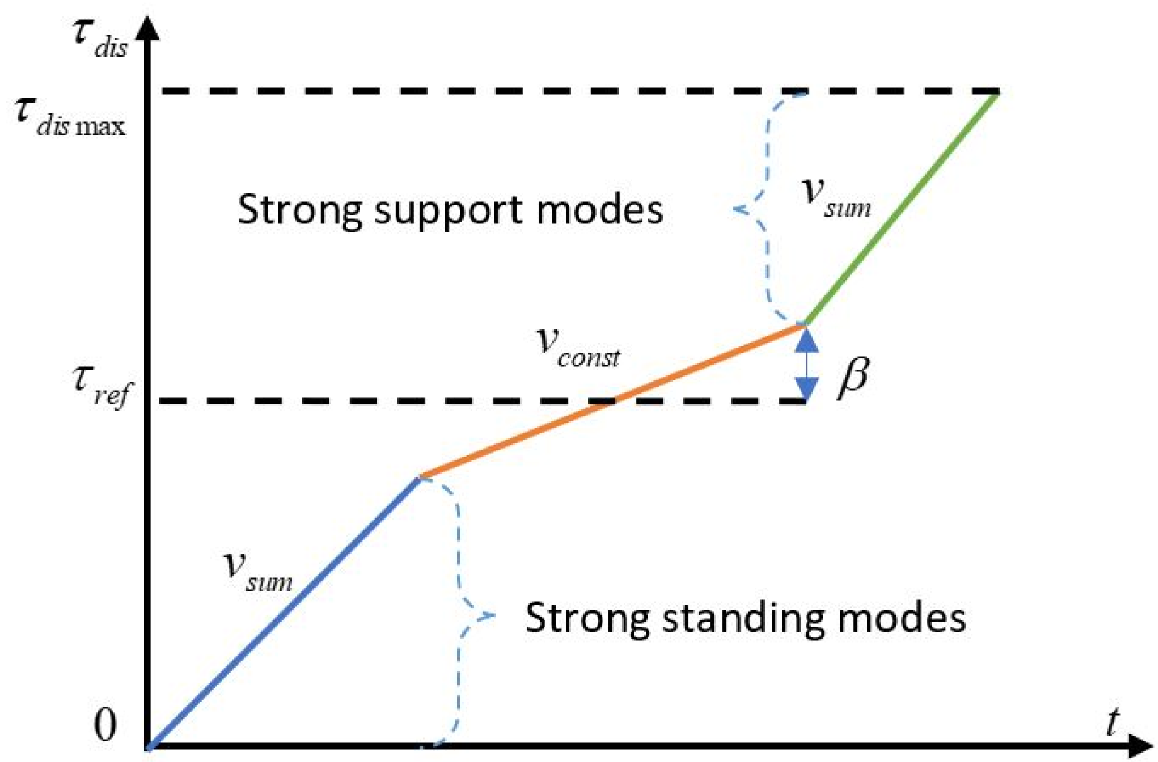

Figure 3.6: Block diagram of the switching modes.

By this smart switching modes based on the nonlinear disturbance observer, we can smart switching between each modes to control the robotic cane to follow the behaviors of the users more comfortable.

3.7 Image Processing Application to Determine the Navigate Line of the Blind

My idea is to develop the robotic canes not only help the users maintain balancing but also support the blind people to walk by using an image processing algorithm to determine the navigate lines.

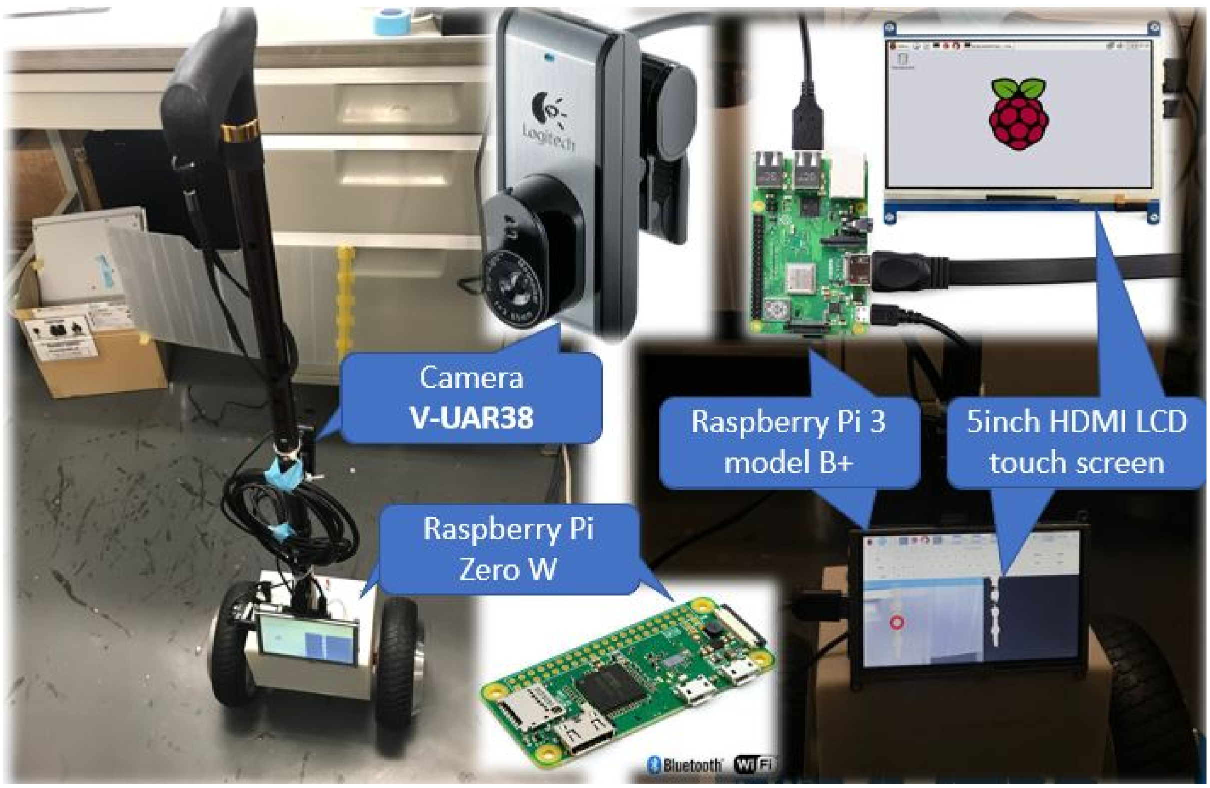

Figure 3.7: Two-wheeled cane including image processing module to support the blind to walk.

The structure of the system can be detailed as shown Fig. 3.7. By using only basic camera mounted on the body of the robotic cane is connected to the Raspberry Pi 3 Model B+ by USB interface to process input images through color detection algorithms to determine the colors of the navigate lines for blind people. The output results of the image processing data is transferred to the center controller of the robotic canes through the UART interface with high-speed transportation lines.

The color detection algorithms can be basic methods because the navigate lines for blind people are fixed defined style depending on the countries. For example, in Japan, yellow color is chosen with some types of lines, but the color is no change. As shown in Fig. 3.8, the center of the navigate lines can be found by image processing method as Object in details.

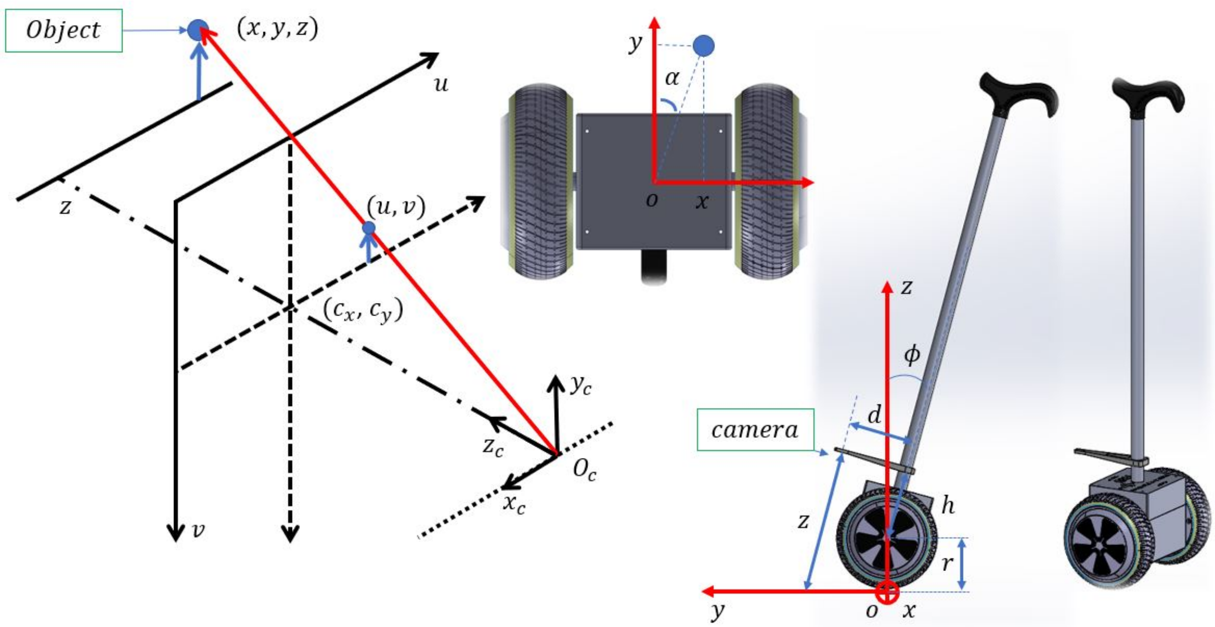

Figure 3.8: System coordinate transformation of the image processing method on the robotic canes.

Moreover, to achieve the results of the determined navigate lines, we also can apply the comparison method to compare the detected lines with the reference line or real images, and then, the true styles of the lines with some important information is utilized to control the robotic canes more clearly.

As shown in Fig. 3.8, h is the distance from camera holder to the wheel axis, d is a distance from the rod to the camera, r is the ratio of the wheel, (u, v) are the coordinates of the projection point in pixels, (x, y, z) are the coordinates of a 3D point in the world coordinate space, (c_x, c_y) is a principal point that is usually at the image center, (f_x, f_y) are the focal lengths expressed in pixel units.

The position of the object in the camera coordinate (o_c, x_c, y_c) can be calculated from Fig. 3.9

by the equations as follows:

$$
\begin{aligned}
x_c &= \frac{h_c}{\cos\phi}\frac{(u-c_x)}{f} \\
y_c &= h_c \tan\left(\phi + \arctan\left(\frac{v-c_y}{f}\right)\right)
\end{aligned}
\tag{3.71}
$$

The distance from the camera to the ground is detected h_c related with the angle of the rod of the robotic canes. This value can be calculated as the equation:

$$h_c = r + h\cos\phi + d\sin\phi \tag{3.72}$$

then, we have the position of the object in the robot coordinate (o, x, y) as:

$$
\begin{aligned}
x &= x_c \\
y &= y_c + d_c
\end{aligned}
\tag{3.73}
$$

with d_c is a distance between camera to the z axis, it can be calculate by ϕ as below:

$$d_c = d\cos\phi + h\sin\phi \tag{3.74}$$

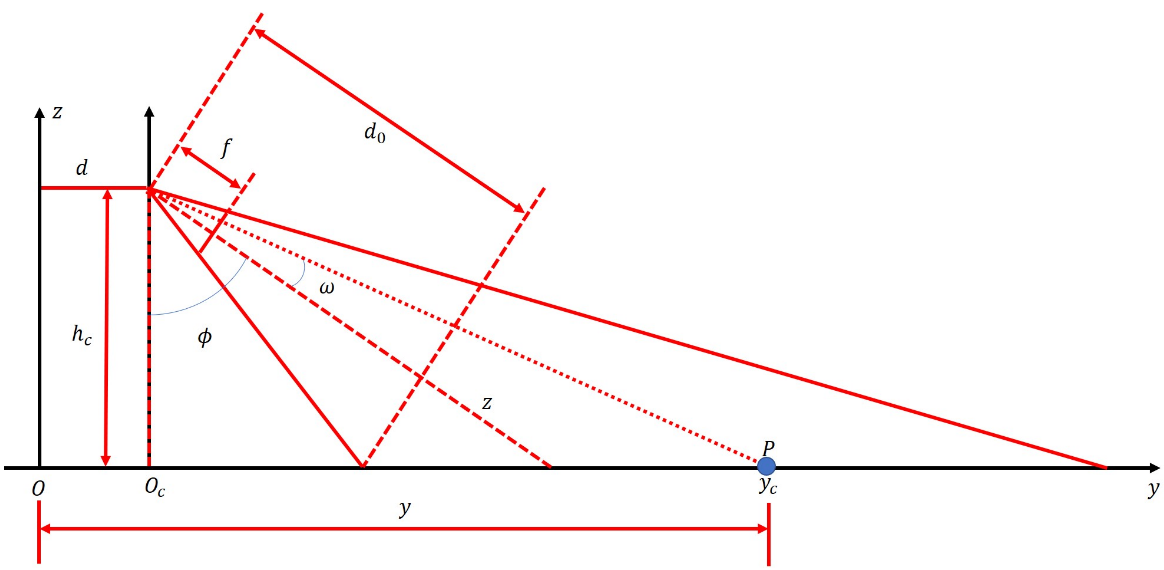

Figure 3.9: System coordinate transfer of the image processing method on the robotic canes.

The angle of the center navigate lines in the coordinate of the robotic cane α can be calculated by:

$$\alpha = \arctan\frac{x}{y} \tag{3.75}$$

The *PD* controller can be approximated as below with *dt* is the sampling time of the *PD* controller of 1s.

$$P = \alpha_{new} \tag{3.76}$$

$$D = \frac{(\alpha_{new} - \alpha_{old})}{dt} \tag{3.77}$$

$$u_{PD} = K_P P + K_D D \tag{3.78}$$

By using *PD* controller, we can re-calculate the input signals of the center controller as below:

$$u = \frac{v - L_f^4 h(x)}{L_g L_f^3 h(x)} + u_{PD} \tag{3.79}$$

3.8 Summary

A mathematical model of the robotic canes based on the inverted pendulum model was proposed in this chapter. The LAM combined with some functions to the controller as a low-pass-filter and smart switching modes is presented in detail. Moreover, the NDOB was analyzed and applied to the proposed controller to find the external human force put on the robotic cane to control the motion of the system depending on the user behaviors. The difference between simulation results and experiments in the previous study was solved successfully on the experiments on the real model in this research by using the gain scheduling and the low-pass-filter.

In addition, the LAM combined with the NDOB and smart mode switching can control the motions of the robotic cane more smoothly and comfortable for users. Moreover, the image processing method is applied to the system to determine the navigate line of blind people. The PD controller is utilized to control the motions of the robotic canes to support blind people to walk in unknown environments.

Thanks to our proposed methods applied to the robotic canes, the motion control of the system is improved greatly, this makes the robotic canes more practical and useful for walking assistance in the near future.

Table 3.2: Definition of symbols

Definition	Symbol	Unit
Rotational kinetic energy of wheel	T_1	J
Rotational kinetic energy of rod	T_2	J
Translational kinetic energy of wheel	T_3	J
Translational kinetic energy of rod	T_4	J
Kinetic energy total	T	J
Potential energy total	V	J
Inertia of rod	J_ϕ	kg·m^2
Inertia of wheel	J_θ	kg·m^2
Viscous friction coefficient of rod	D_ϕ	N.m.s/rad
Viscous friction coefficient of wheel	D_θ	N.m.s/rad
Length of rod	l	m
Center of mass of rod	l_c	m
Mass of rod	m	kg
Mass of wheel	M	kg
Actuation torque	τ	N.m
Actuation torque on the right motor	τ_R	N.m
Actuation torque on the left motor	τ_L	N.m
Gravitational acceleration	g	m/s^2
Radius of wheel	r	m
Angle of the rod	ϕ	rad
Angle of the wheel	θ	rad
Disturbance according to ϕ	d_1	Nm
Disturbance according to θ	d_2	Nm

Chapter 4

Performance Evaluation and Comparison of the Robotic Cane by Simulations and Experiments on the Real Models

4.1 Abstract

The performance of the robotic cane will be evaluated in this chapter. The performance of the robotic cane utilizing the LAM is compared with that of another methods like the traditional LQR method in controlling the inverted pendulum model. The stability of the system is required to follow the rule that the angle of the rod of the robotic cane should be close to the equilibrium point of 0 rad, and the position of the robotic cane should follow the angle response of the robotic cane. Moreover, due to the ratchet structure, the robotic cane can support the user with a strong stability without any problem in the emergency modes. Next, we do more experiments on the real designed model of the robotic cane in basic environments and slope environment.

The root mean square error (RMSE) is adopted as the performance index because it shows the stability or the precision of the proposed controller. This is very essential to control the robotic cane while it supports the user to stand or to walk. When the system is stable, the robotic cane operates properly with its main functions which is to support the user without any vibration on

the system. Although the RMSE is not full enough for evaluating the function of the robotic cane, it can evaluate the stability when the cane supports the user to maintain balancing. Detail in formation wil be discussed through my experiment results in next sections.

The reference value of the RMSE is determined based on the functions of the robotic cane: In self-balancing mode: the reference value of the RMSE should be zero in both sides of the angle and the position of the robotic cane based on the stability of the inverted pendulum model; To evaluate the response to sudden disturbance: the reference value of the RMSE is the value getting from the real force sensor; in other cases, the reference value of the RMSE can be determined depending on the state of the robotic cane while it supports the user.

The hardware of the robotic cane and its controller were presented in the Chapter 2 and Chapter 3. This section analyzes the experiment results and simulation results on the designed hardware of the robotic cane.

In the experiments, we propose specification rule of the controller to make the robotic cane safety for the user as follows:

- The robotic cane can strongly support the user maintain balancing between -0.5 rad and $+0.5$ rad.
- The largest working range of the robotic cane angle from -0.25 rad to $+0.25$ rad.
- The feedback velocity of the robotic cane reacts to the user's behaviors between -0.3 m/s and $+0.3$ m/s. This velocity is limited by the special needs of older users.

4.2 3D Simulation

In both 3-D simulations and tests, the self-balancing mode of the robotic cane is first considered. Next, the response of the robotic cane is discussed when the robotic cane helps the real users maintain balancing.

A 3-D model of the robotic cane is composed by the C/C++ language built on the Raspbian OS. The simulation results when LAM and the NDOB are applied were strongly stable round the equilibrium point (Fig. 4.1-4.2).

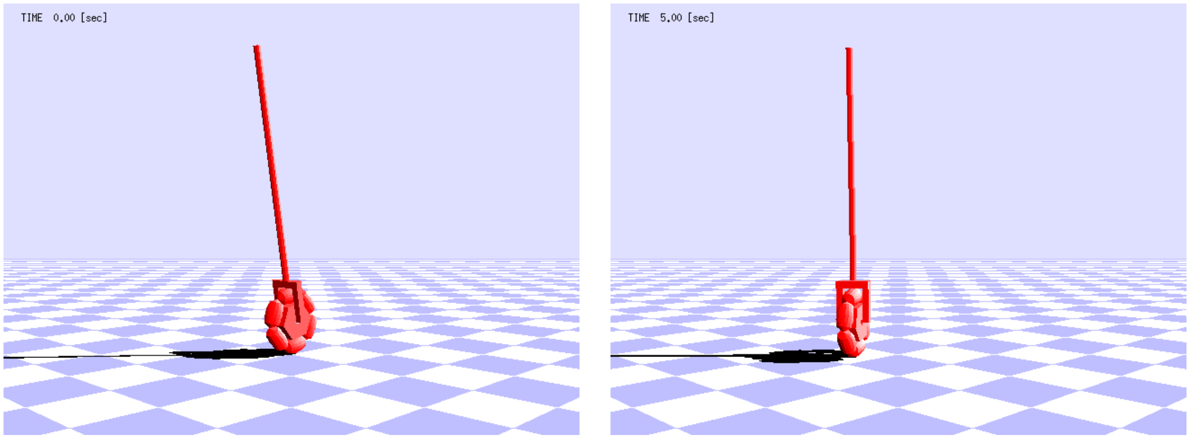

a) b)

Figure 4.1: Robotic cane in the self balancing mode: (a) initial position at 0.17 rad; (b) position after 5 s.

As shown in Figs. 4.1-4.2, after reaching the equilibrium point of 0.0 rad at 1.5 s from the initiation point of 0.17 rad, the robotic cane remains strongly stable in the last period with very small vibrations round the balancing point.

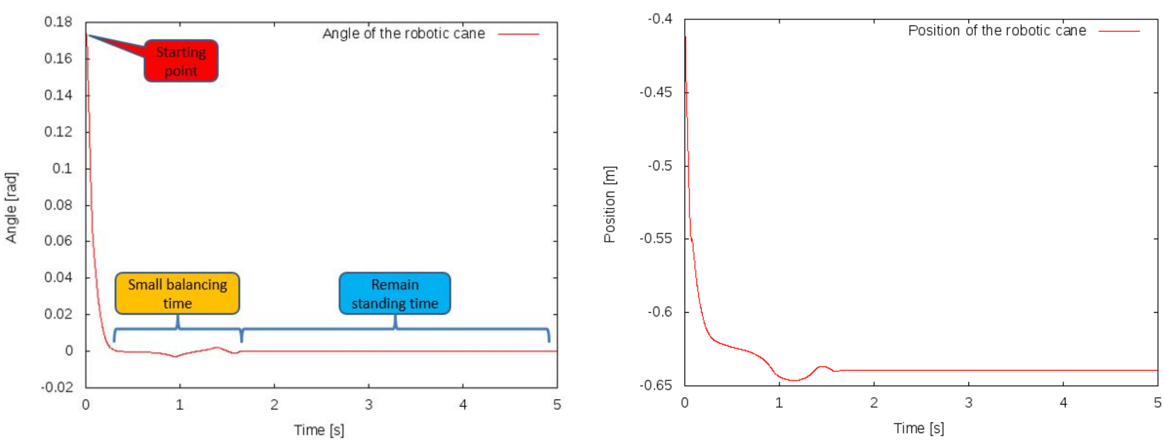

a) b)

Figure 4.2: The angle and the position of the robotic cane in self-balancing mode on the sagittal plane: (a) Angle (b) Position.

In detail, with a small vibration of ±0.005 rad in the first period, the robotic cane can approach the equilibrium point after 0.3 s with the starting point of 0.17 rad as shown in Fig. 4.2 (a).

Fig. 4.2 (b) shows that the position of the robotic cane responded more quickly from −0.42

m to −0.62 m throughout the identical initial time before being strongly stable around the equilibrium position of −0.63 in the last period.

4.3 Performance of LAM Compared with LQR Method on the Real Hardware of the Robotic Cane

The nonlinear systems of the inverted pendulum model is stabilized by the LQR method which is the popular method was proposed in [13, 14]. However, this method just can linearize the nonlinear system close to the zero degree, this does not meet requirements for the robotic cane when it supports the user maintain balancing. This working angle must be bigger than the zero degree.

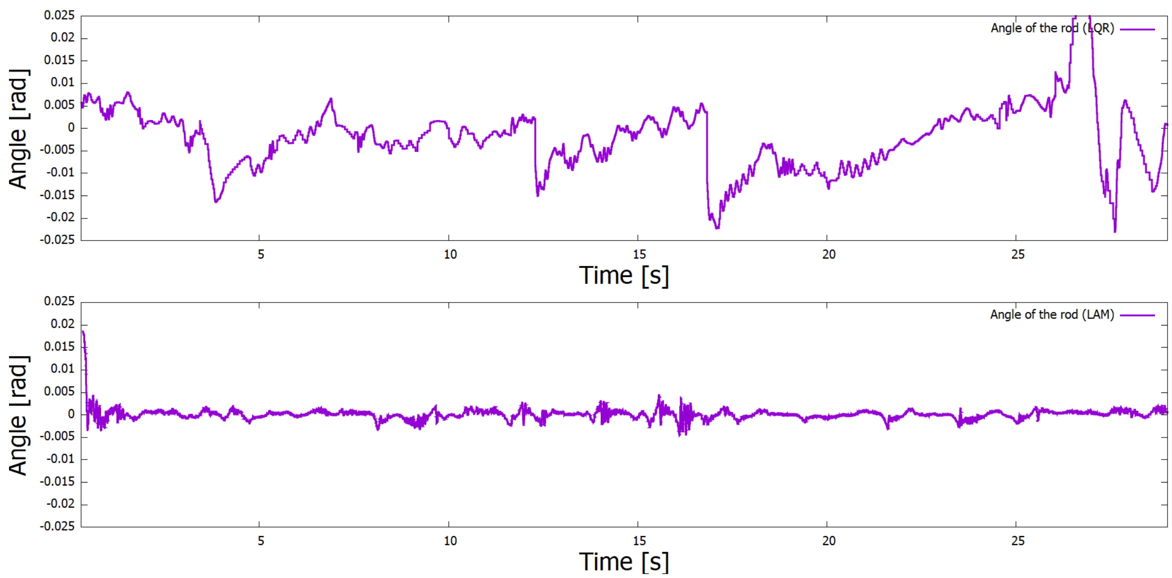

Figure 4.3: Angle of the robotic cane in self balancing mode: the LQR method (top) and LAM (bottom).

The LQR cost equation is defined as (4.1):

$$J(u) = \int_{0}^{\infty} (x^T Q x + u^T R u) dt \tag{4.1}$$

The optimal controller is given by (4.2), where K is the matrix gains of the controller:

$$u(t) = -Kx(t) \tag{4.2}$$

To reused the LQR method, simple approximation the parameters of the robotic cane is taken as $\phi = 0$ gives $\sin\phi = \phi$, $\cos\phi = 1$, and $\dot{\phi}^2\phi = 0$.

The response angle of the robotic cane by LAM (bottom) is compared with LQR method (top) on the sagittal plane as shown in Fig. 4.3. Specially, starting from 25 s to the end of the period, the robotic cane applied the LQR method was unstable while the LAM remains strongly stable of 0.0 rad.

The RMSE index is 0.00344 with LAM and 0.05675 with LQR method, shown that our LAM is the higher performance than other methods.

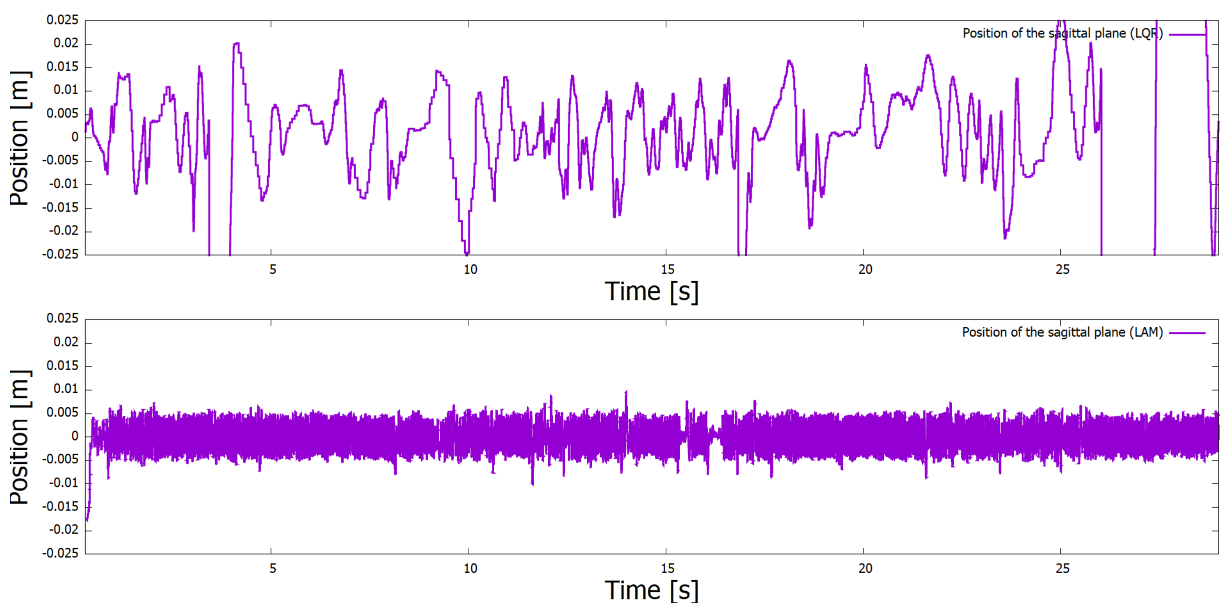

Figure 4.4: Position of the robotic cane in self-balancing mode on the sagittal plane: the LQR method (top) and LAM (bottom).

Next, the excellent performance of LAM compared with LQR is proved by the response of positions of the robotic cane. As shown in Fig. 4.4, the robotic cane was in self-balancing mode at 0.0 rad without any vibrations by LAM while this value was significantly fluctuated around -0.05 m and 0.05 m until 25 s and became unstable in the last period.

4.4 Extended Experimental Results of the Controller

In this section, the experiment results on the real device of the robotic cane are presented.

The robotic cane is strongly self-balancing around the equilibrium point by using LAM with the internal battery as shown in Fig. 4.5 (a). The robotic cane operates within 30 minutes before the battery needs to be charged by utilizing the only internal battery. However, when the external battery is included, the robotic cane can work continuously more than 2 hours.

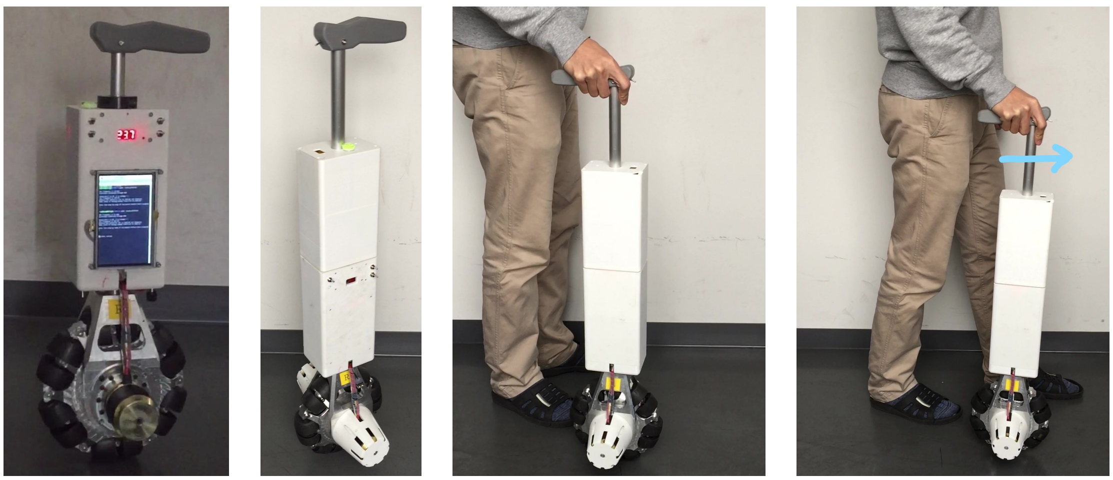

a) b) c) d)

Figure 4.5: The working statuses of the robotic cane: (a) self-balancing without the external battery; (b) self-balancing with the external battery; (c) support the user while standing, and (d) help the user walk in the sagittal plane.

As shown in Fig. 4.6 (a), the fluctuation angle of the robotic cane in the sagittal plane is ±0.01 rad, while this value is only from −0.006 to 0.001 rad in the lateral plane with the initial angles of −0.32 rad and −0.12 rad in the sagittal and lateral planes, respectively.

The position of the robotic cane has a small vibration at around ±0.01 m in the sagittal plane while this value is nearly 0 m in the lateral plane in Fig. 4.6 (b). These results prove that LAM combined with the NDOB makes the robotic cane more strongly stable around the equilibrium point without any external supporter for a long time.

Moreover, the robotic cane supports the user to stand (Fig. 4.5 (a)) and to walk (Fig. 4.5 (b)) by grasping the grip handle.

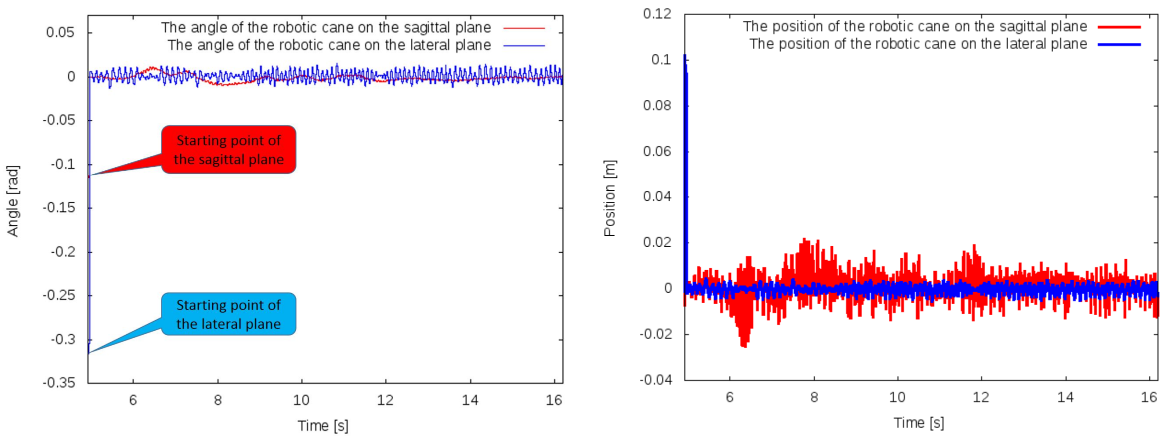

a) b)

Figure 4.6: The robotic cane is self-balancing around the equilibrium point in the lateral (blue) and sagittal (red) planes: (a) the angle; (b) the position.

To support the user to substantially walk in Fig. 4.5 (d), the user only needs to put a small force to control the motions of the robotic cane going toward or backward or turning to the left and right positions.

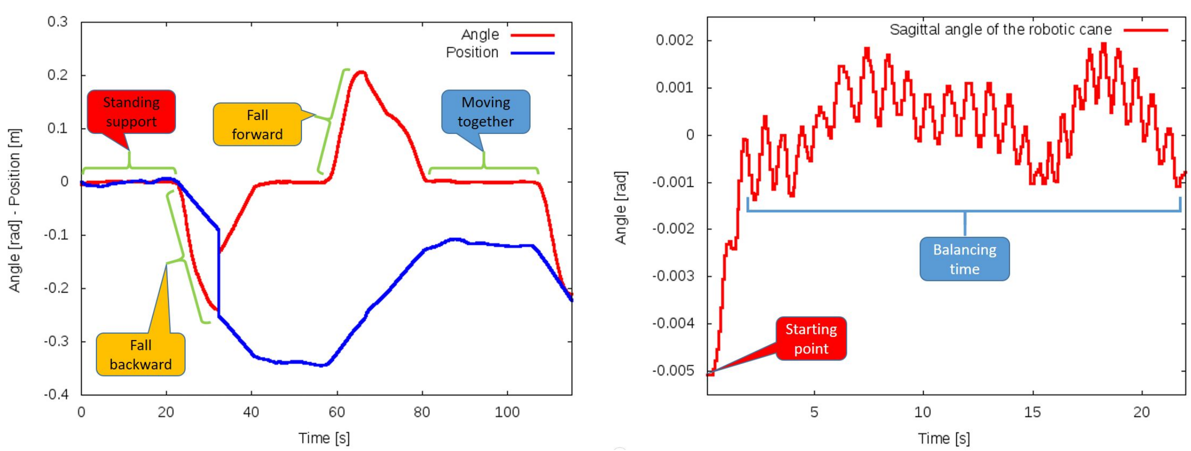

a) b)

Figure 4.7: The robotic cane helps the user fall prevention: (a) the angle and the position; (b) the zoom-in angle from 2.5 to 22 s.

The performance of the robotic cane can be determined by the response of the robotic cane with the behaviors of the user as shown in Fig. 4.7 (a). In the period of 2.5 and 22 s, the robotic cane vibrated only around ±0.0015 rad while support the user stand substantially (see Fig. 4.7

(b)).

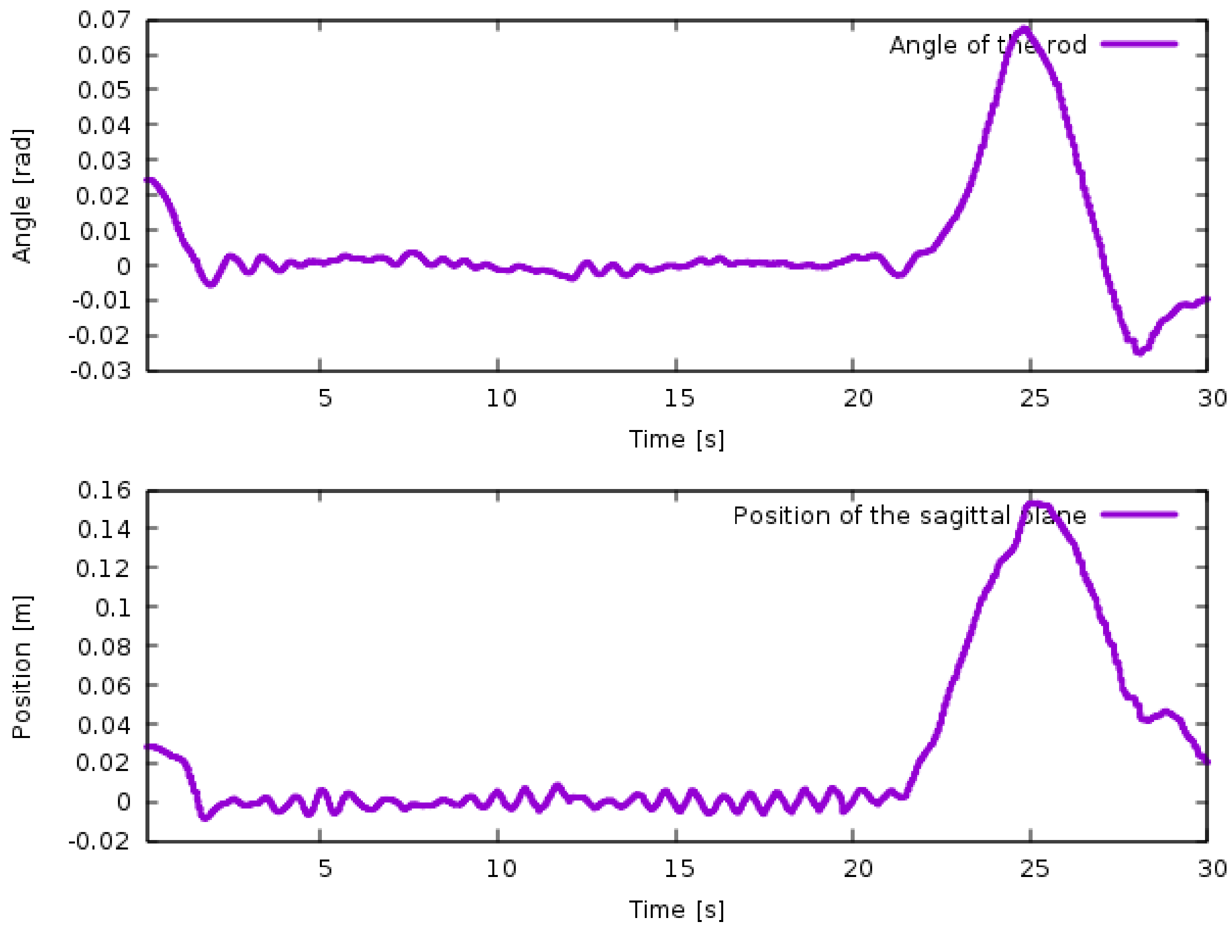

Figure 4.8: The robotic cane supports the user to stand and to walk: (top) the angle; (bottom) the position.

As shown in the top of the Fig. 4.8, the robotic cane can approach the equilibrium point after only 2 seconds with the starting angle of around 0.025 rad. In the next period from 2 to 20 seconds, the robotic cane supports the user to substantially stand at the equilibrium point. When the user applies a small force to the robotic cane in any directions, that means the user needs support from the robotic cane in that direction to walk. For example, from 20 s to 25 s the robotic cane moved simultaneously together the user.

The robotic cane responded more quickly depending on the user's behaviors as being to fall backward (Fig. 4.9 (a)) before returning the user to the stable position (Fig. 4.9 (b)), corresponding to the period from 22 s to 35 s in Fig. 4.7 (a).

a) b) c) d)

Figure 4.9: The robotic cane supports the user to prevent falling: (a) fall backward, (b) restore the user's new balance, (c) fall forward, (d) restore the user's new balance.

Similarly, the robotic cane adjusted its position by itself to help the user get back a new standing position in Fig. 4.9 (d) after the user began to fall forward in Fig. 4.9 (c). The response of the robotic cane's angle with its position is detailed from 60 – 80 s in Fig. 4.7 (a).

To prove the effectiveness of the robotic cane on the user, we implemented the experiments on different objects with the gyroscope sensor mounted on the body of the users as shown in (Fig. 4.10).

In the top of Fig. 4.11, the body vibrations were the largest when the users to walk without any supported device from -10 to 0 μT and the users need the biggest energy for walking.

As shown in the Fig. 4.11 the RMSE index when the user walks without any supporter is 2.297568, this value is reduced a litter bit to 2.041593 with support by the traditional cane while it had a great decline to 0.838351 when the robotic cane is used with the center vibrations of -4.5 uT, -5.5 uT, and -1.75 uT respectively. That values indicate that the proposed robotic cane has the high performance to support the user to walk and to stand than the other devices.

The users used the traditional cane (center panel of Fig. 4.11) to walk, but the body of the users still fluctuated between -9 and 0 μT when the cane was lifted off the ground, the user did not received any suppor in this period.

In contrast, the user's vibrations are the smallest vibrations of -4 and 1 μT while the robotic cane is used for the walking assistance (bottom panel of Fig. 4.11). In this case, the user needs much smaller energy to walk than other cases.

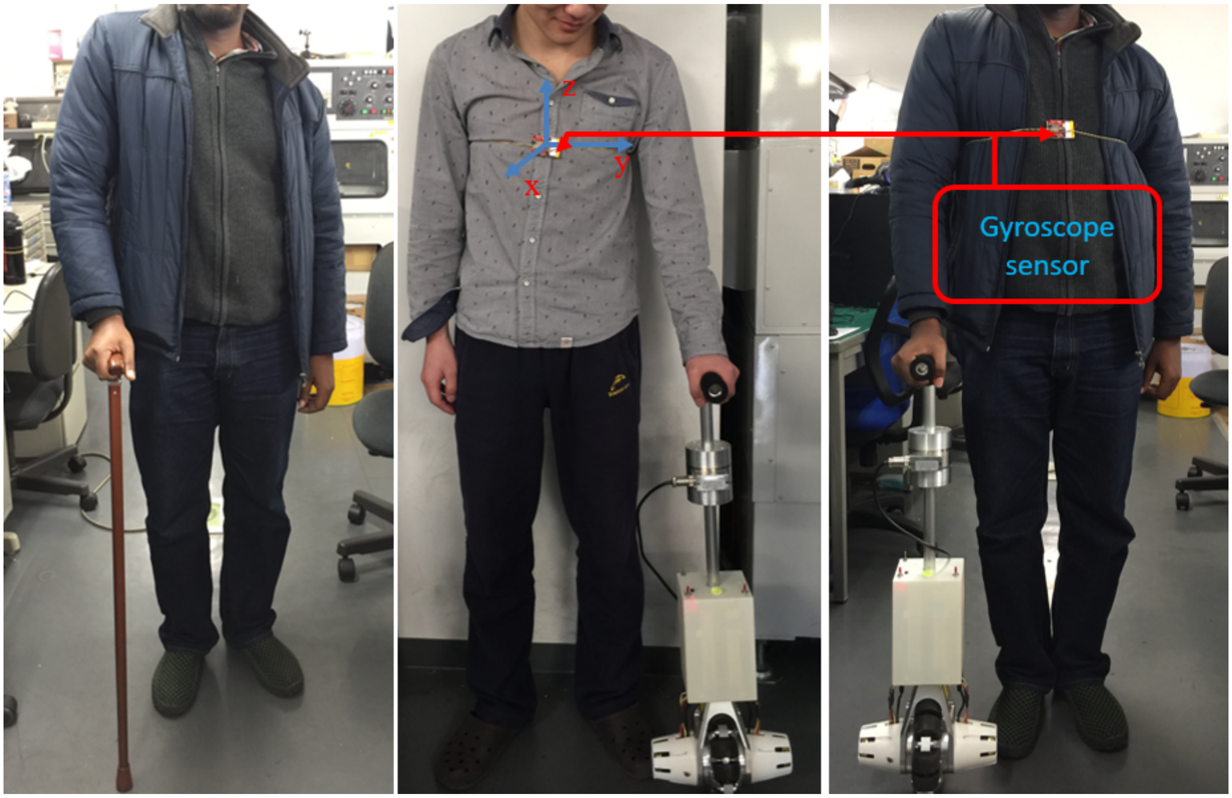

Figure 4.10: The user is supported by a traditional cane (left) and the robotic cane (center and right) with the body measurement module attached.

Table 4.1 shows the body vibration magnitudes of the users, these values are determined by the gyroscope sensor mounted on the body in three user states: without support, supported by a traditional cane, and supported by the robotic cane.

The results on the other subjects are also shown in Tab. 4.1. The robotic cane eliminated the body vibrations in the cases of ”no support” and ”traditional cane” by 3.12 times and 2.48 times, respectively. From the results, it can be also seen that the balance support performance of the LAM combined with the NDOB on the robotic cane does not almost depend on the age of the user.

Table 4.1: Body measurements of the users in the lateral plane: without supporter, traditional cane, and the robotic cane.

Subjects	Without supporter (μT)		Traditional cane (μT)		Robotic cane (μT)	
	Min	Max	Min	Max	Min	Max
1	-10	0	-9	0	-4	-1
2	32	41	20	28	22	26
3	-24	-10	-25	-17	-16	-13
4	-21	-9	-12	-2	-5	-8
5	12	29	11	20	13	18
6	29	35	30	35	32	34
7	2	12	5	11	4	7
Average	11.14		8.86		3.57	
Subjects	Gender	Age[Years]	Weight[Kg]		Height[m]	
1	Male	28	55		1.68	
2	Male	30	62		1.72	
3	Male	25	56		1.62	
4	Male	27	53		1.70	
5	Male	32	58		1.75	
6	Male	31	68		1.67	
7	Male	26	60		1.60	

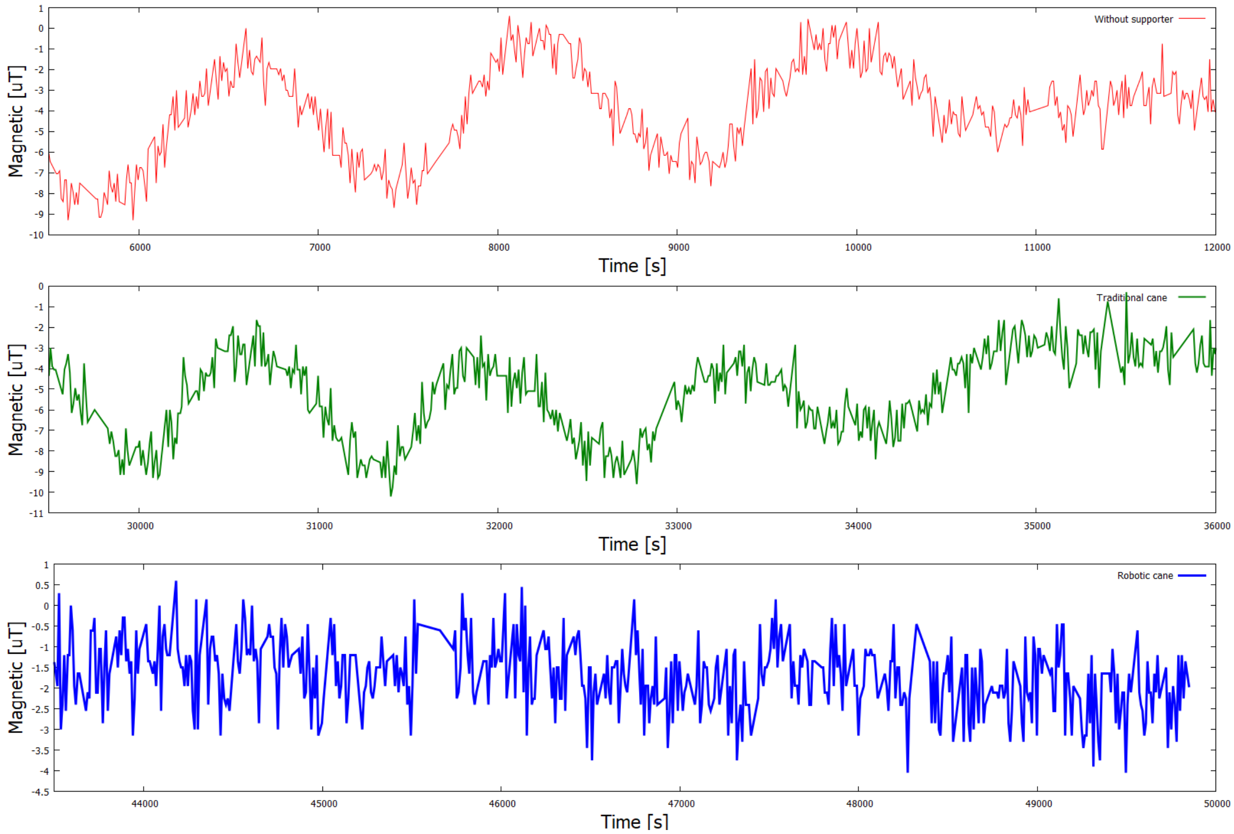

Figure 4.11: The users to walk with no support (top), a traditional cane (middle), and the robotic cane (bottom).

4.5 Smooth Mode Switching Method

In the self-balancing state, the robotic cane slightly vibrated around the equilibrium position (1 - 13 s in Fig. 4.12). This vibration may cause the design error of the gearbox and the high-gain controller.

We propose two methods to suppress this vibration:

- Firstly, in the mechanic design we attach a touch sensor on top of the handle (Fig. 2.1). By using this touch sensor we can switch between each mode easier than other methods. When the user grasped the handle with the touch sensor, the vibration was completely canceled (as shown from 13 s in Fig. 4.12), and the robotic cane will change to the assistance mode.
- The second way is use of software methods like using smart switching mode method as

presented in the previous sections. We can control and switch modes automatically without touch sensors. Depending on the estimated external force applied to the rod of the robotic cane by using NDOB and the behavior of the user, the controller of the system will control the motions of the robotic cane for walking assistance or standing by only automation switching modes of the controller.

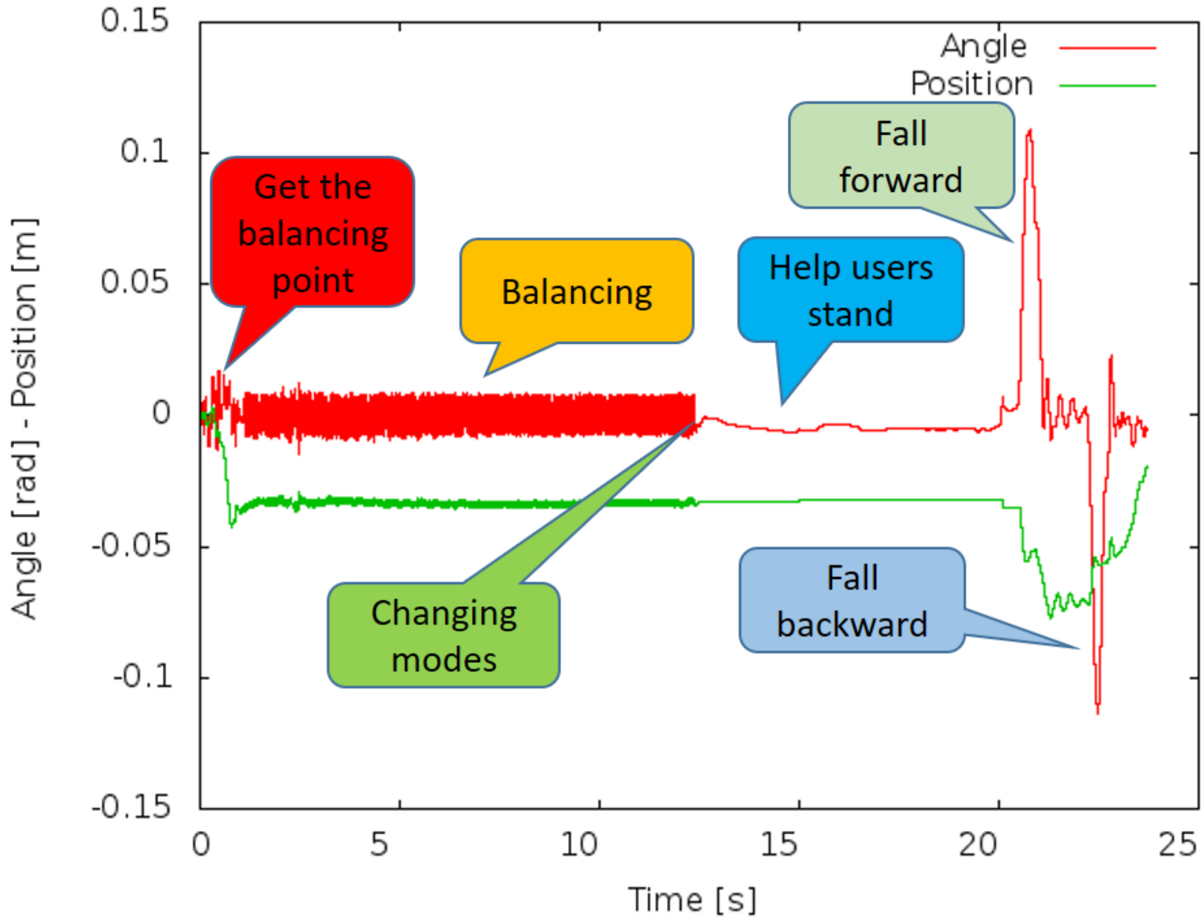

Figure 4.12: Mode switching to support the user to maintain balancing by using a touch sensor.

4.6 Evaluation Performance of the Controller on the Slope Environments

The performance of the controller of the robotic cane will be verified agin in this section based on the experiments of the real device on the slope environment. Uneven surfaces are always a major obstacle to devices that support people to move. Especially steep and rugged roads, where mobility aids for the elderly are almost inoperative or inefficient. Slope environments where experiments are done are shown in Fig. 4.13 with the angle of the slope is about 22 degree.

Figure 4.13: Experiment of the robotic cane on the slop environment.

Fig. 4.14 (a) shows that the device supports the user to be strongly stable with the angle of the rod of the robotic cane in the sagittal plane around 0.06 rad from 100 s to the end of the period. The angle vibration is 0.034865 rad is calculated by RMSE index. That value is closed to 0 rad of the equilibrium point of the inverted pendulum model. Following this behavior of the user, the positions of the robotic cane in the sagittal plane describe that this device supported the user step by step climb the slope without any problems while keeping the angle of the rod to be strongly stable together with the user.

Fig. 4.14 (b) also indicated that the angle of the rod of the robotic cane in the lateral plane almost has no change with the vibration from −0.03 rad to 0.04 rad and these values are closed to the equilibrium point of the inverted pendulum model.

The positions of the robotic cane in this plane shown that the user climbs the slope in the straight line without any vibration on the left and the right side.

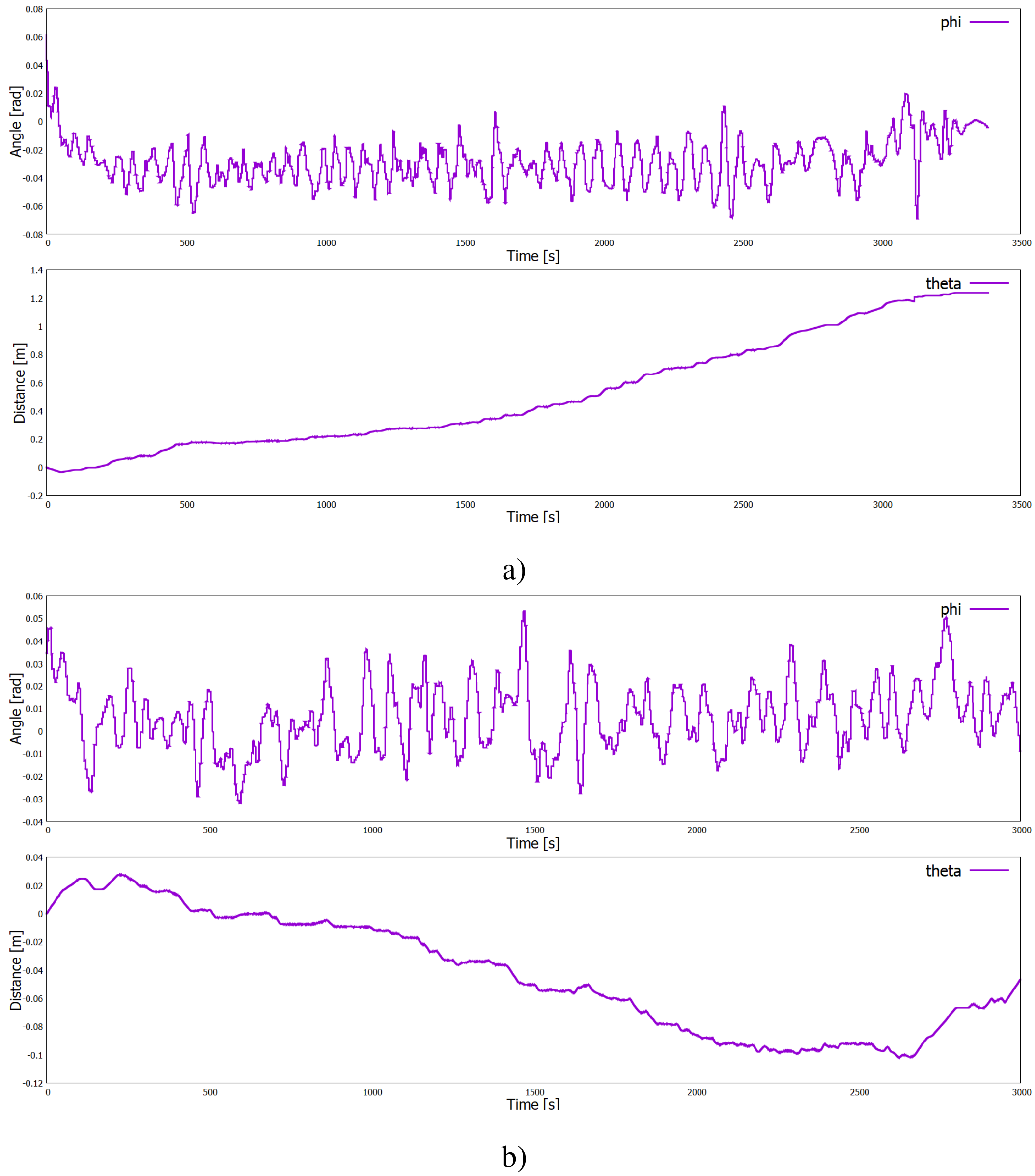

Figure 4.14: The angle and the position of the robotic cane supports the user to walk on slope environment in sagittal and lateral plane.

In the lateral plane, Fig. 4.14 (b) shows that the robotic cane has no fluctuations with the user while supporting the user to walk on the slope environment (the top of the figure).

The positions of the robotic cane just has a small vibration while the user climbs the slope environments (the bottom of the figure) without any problems.

4.7 Summary

In this chapter, the performance of the robotic cane was verified. The proposed controller applied to the robotic cane for walking assistance was proved that it controls the motions of the robotic cane very effectively. The user is supported to be strongly stable when he moves with the robotic cane together in any environment conditions.

Firstly, the 3D simulation has shown that our controller applied to the robotic cane can make the system strongly stable without any problems, the angle of the robotic cane is close to the equilibrium point of the inverted pendulum model. Moreover, the performance of the nonlinear controller deployed on the robotic cane is demonstrated through the comparison with the LQR method, these results showed that our controller is much better than the other methods.

Secondly, when the proposed controller deployed the real model of the robotic cane, the experimental results indicated that the system is strongly stable around the equilibrium point and very useful to support the user maintain balancing. Moreover, thanks to smart mode switch by a touch sensor, we can control the system more comfortable than only use one gain to control the device to support the user to maintain balancing as the traditional methods.

Finally, the excellent performance of the LAM applied to the robotic cane was proved by experiments on the slope environment where the angle results is close to the equilibrium point of the inverted pendulum model.

Chapter 5

Extended Experiment Results on the Two-Wheeled Cane and the Two-Wheeled Walker

5.1 Abstract

The chapter tests the performance of the LAM algorithm through experiment results test on the two-wheeled cane and the two-wheeled walker. The performance evaluation of the controller is verified again by the experiments on the slope environments. Moreover, application of image processing algorithms to determine the navigate line to support the blind people to walk will be presented in detail.

5.2 Two-Wheeled Cane

5.2.1 Self-Balancing of the Two-Wheeled Cane

Firstly, the two-wheeled cane is able to be self-balancing with or without a supporter in the primary working modes of the inverted pendulum model.

a) t = 10.0 s   b) t = 900.0 s

Figure 5.1: Self-balancing mode of the two-wheeled cane.

All of the experiments with the two-wheeled cane was stored by videos and a several of pictures as shown in Fig. 5.1.

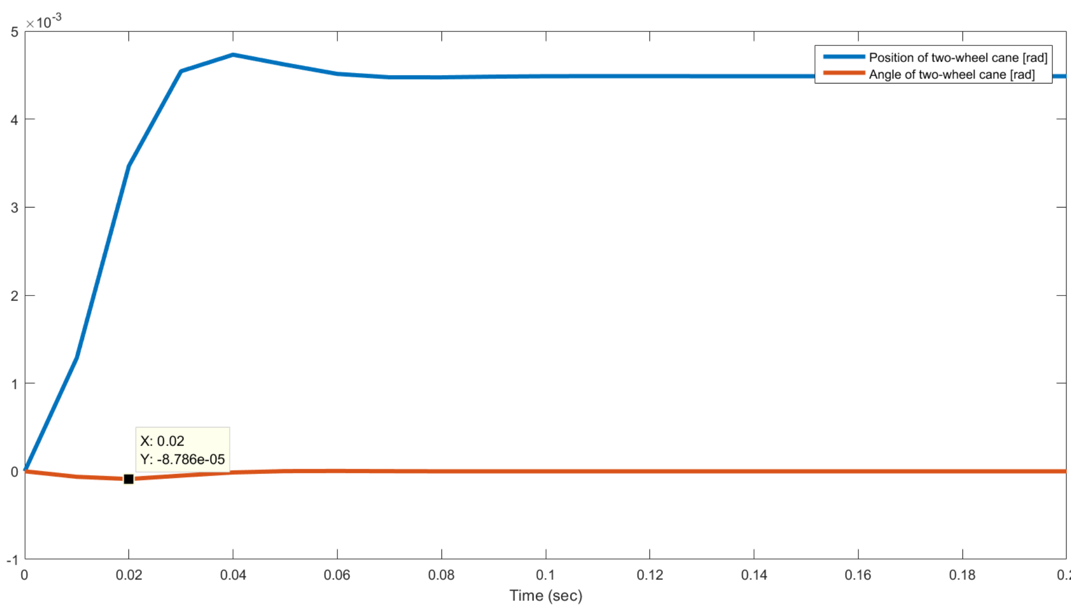

Figure 5.2: Angle of the two-wheeled cane while balancing by itself.

In Fig. 5.2, the two-wheeled cane approached the equilibrium point after only 0.05 s with the angle of the rod of 0.00008786 rad at 0.02 s and keeps still at 0 rad in the last period. After only 0.02 s, the two-wheeled cane can get the equilibrium point and strongly stable by itself without any vibration in the last period.

This result demonstrates that using the LAM can linearize the nonlinear system not only around the zero point like the LQR method, but also around large tilt angles of the two-wheeled cane.

5.2.2 Nonlinear Disturbance Observer Estimation

When the user intends to fall forward from 0.7 s to 0.8 s, the human force put on the rod of the two-wheeled cane is positive and 0.06 N in the head direction of the two-wheeled cane. Similarly, when the user intends to fall backward, the human external force measured by torque sensor has a negative value, e.g..0.05N. The NDOB is estimated from 0.8 s to 0.9 s. The performance of the NDOB is expressed by the smoothy line with no noise and vibration as shown in Fig. 5.3 with the error of less than 5%.

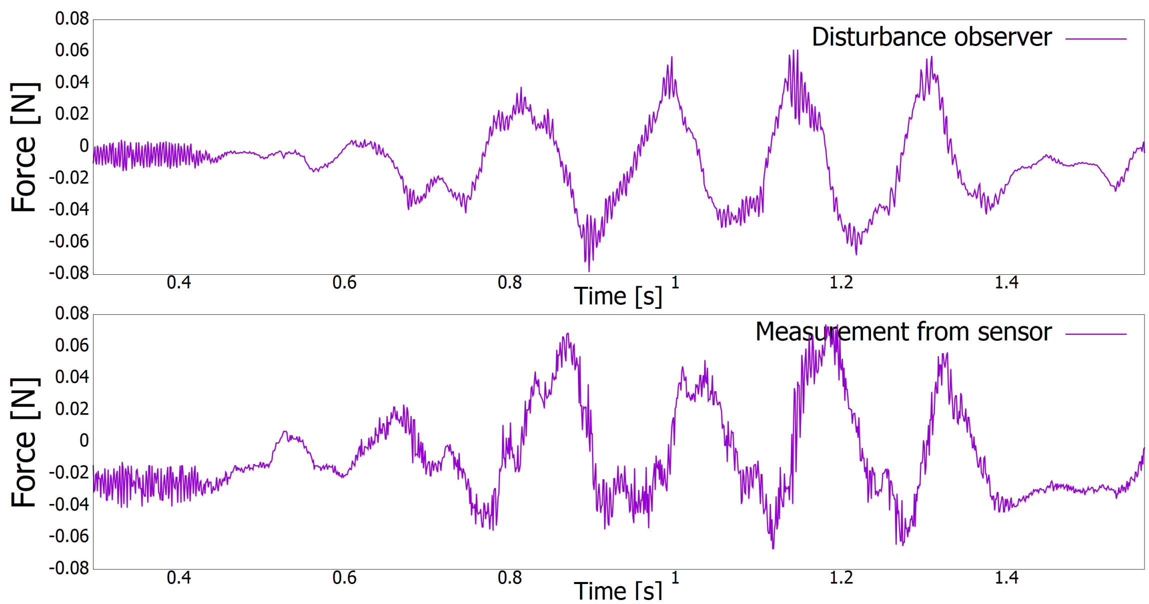

Figure 5.3: Estimated torque by NDOB and measured torque by the torque sensor on the two-wheeled cane.

In Fig. 5.3, the NDOB which is used to estimate the human external force put on the two-wheeled cane achieves the same result like the torque sensor installed on the rod in all periods of the three cases: standing, fall forward and fall backward.

5.2.3 Support the User to Walk

Figure 5.4: Another cases of the two-wheeled cane to help the user to walk.

In the next evaluation, the performance of the two-wheeled cane using LAM combined with the NDOB expressed by the angle and response position of the two-wheeled cane is discussed in Fig. 5.5.

Three cases are considered as shown in Fig. 5.5:

- Firstly, when the user needs to keep balanced from 0 rad to 2.2 rad in the first period. In this case, the two-wheeled cane supports the user approach a balancing point through the grip handle. The angle and the position of the two-wheeled cane oscillates around the equilibrium point of 0.01 rad and 0.04 m, respectively.

- The second case is when the two-wheeled cane aids the users to walk. The position of the two-wheeled cane is determined by the angle of the rod compared to the equilibrium point and the estimated torque put on the rod creates a suitable position to aid user keep balancing while they are going from 2.2 s to 2.6 s.

- Finally, as displayed in the last period, when the user tend to fall backward or fall forward, the result reveals that when the angle of the two-wheeled cane is varied to positive or negative values, the positions of the two-wheeled cane will follow correspondingly to support the user reach a new equilibrium point from 2.6s to the final period.

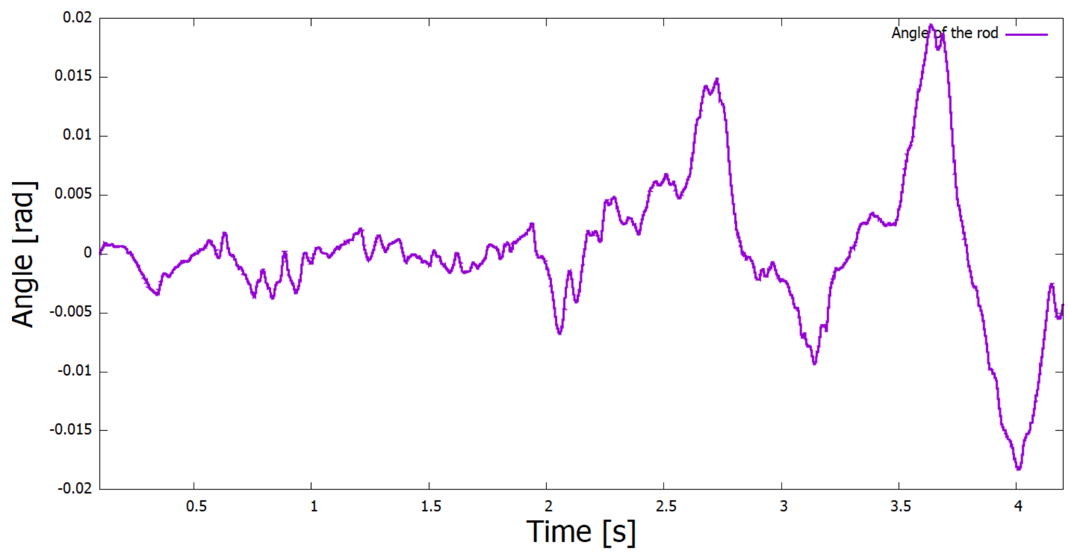

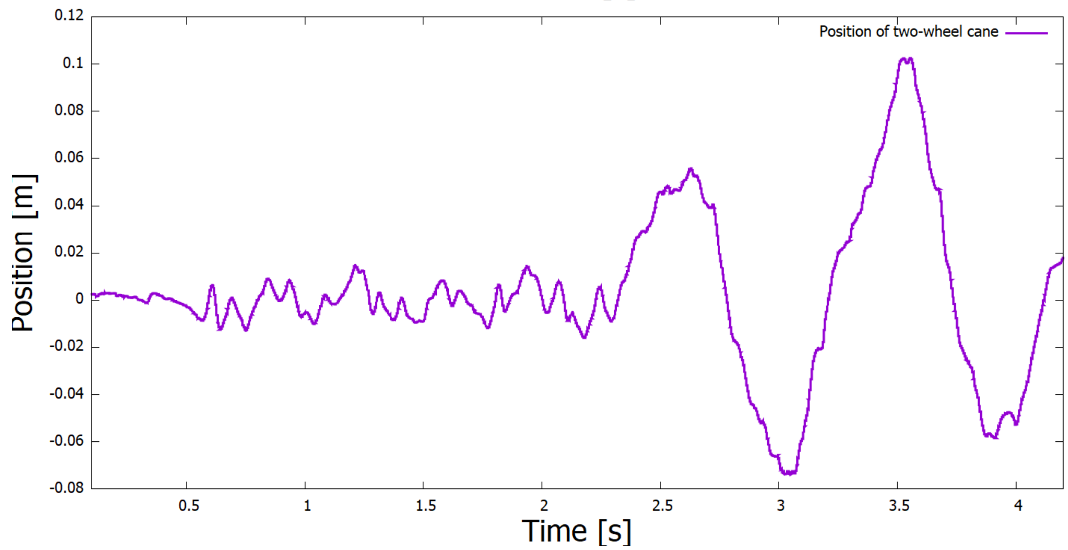

Figure 5.5: The two-wheeled cane helps the user to walk: (top) the angle; (bottom) the position.

In the first case, the torque estimated by NDOB is given in Fig. 5.3. In the early period from 0 s to 0.6 s, both the user and the two-wheeled cane attempt to keep the equilibrium point with the human force fluctuations between −0.05 N and +0.05 N before getting stable in the last period with the human force near the zero point.

Fig. 5.4 shows the results in the second. Depending on the behaviors of the users and the force estimated by the NDOB, a suitable output torque is put to the motor axis and this torque is computed via (3.21) by the torque estimation to support the two-wheeled cane vary the position with a corresponding angle of θ.

a) b) c) d) e)

Figure 5.6: The two-wheeled cane helps the user to prevent falling.

The two-wheeled cane aids the user stand Fig. 5.6 (c). But, in some situations, the user tended to fall backward as shown in Fig. 5.6 (d), and then the robot catches the human force put to the rod of the two-wheeled cane to vary its position to aid the user in reaching a new equilibrium point in Fig. 5.6 (e) (in the final period of 2.6 s to 3 s Fig. 5.5).

Similarly, in the last period of 3 s to 3.5 s in Fig. 5.5, when the user begins to fall forward as shown in Fig. 5.6 (b), the two-wheeled cane aids them stand or keep balancing around the equilibrium position (Fig. 5.6 (a)).

Thus, with the evaluated human force put on the rod of the two-wheeled cane, the controller administer the position and the velocity of the robotic cane to support the user keep their balance while they walk or tend to fall backward or forward.

5.2.4 Experiment on Slope Environment

In this subsection, we present experiments of the two-wheeled can on the slope, with the angle of the slope is around 15 degree, and the distance is around 20 m, more detail information about the environment can be seen in Fig. 5.7.

As illustrated in Fig. 5.7 (a), the two-wheeled cane can balance by itself on the slope. When the user needs to support from the two-wheeled cane, he hold (Fig. 5.7 (b)), and depending on the force put on the device or the angle of the rod, the two-wheeled cane will help the user go toward (Fig. 5.8) as expressed by the blue color line from 1.5 s to the end of the period while remaining strongly stable with the angle of the rod around equilibrium point of 0 rad (Fig. 5.8 - pink line).

a) b)

Figure 5.7: Two-wheeled cane in self-balancing mode (a) and help the user to walk on slope environment (b).

In the similar way, as detailed in Fig. 5.8, the velocity of the rod of the two-wheeled cane in the purple color is around 0.4 rad/s, this value is close to the equilibrium point of 0 rad/s that proves the device to be strongly stable without any problems.

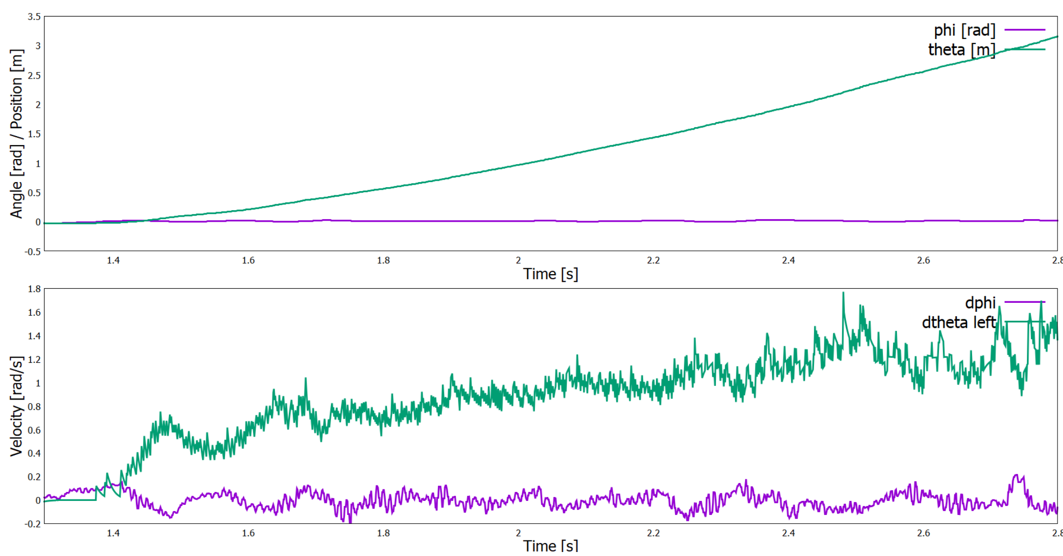

Figure 5.8: The angle and the velocity of the two-wheeled cane while helping the user to walk on slope environment.

Following these behaviors of the user, the velocity of the two-wheeled cane slowly increased because the user went toward without stopping or fell down as shown in Fig. 5.8 (green line).

5.3 Two-Wheeled Walker

5.3.1 Self-Balancing Mode of the Two-Wheeled Walker

a) b)

Figure 5.9: Selft-balancing mode of the two-wheeled walker: (a) at the 1^{st} second; (b) at the 45^{th} second.

Firstly, the two-wheeled cane is able to balance by itself with or without a supporter in the basic working modes of an inverted pendulum model.The two-wheeled walker is strongly stable around the equilibrium point in the self-balancing mode as shown in Fig. 5.9.

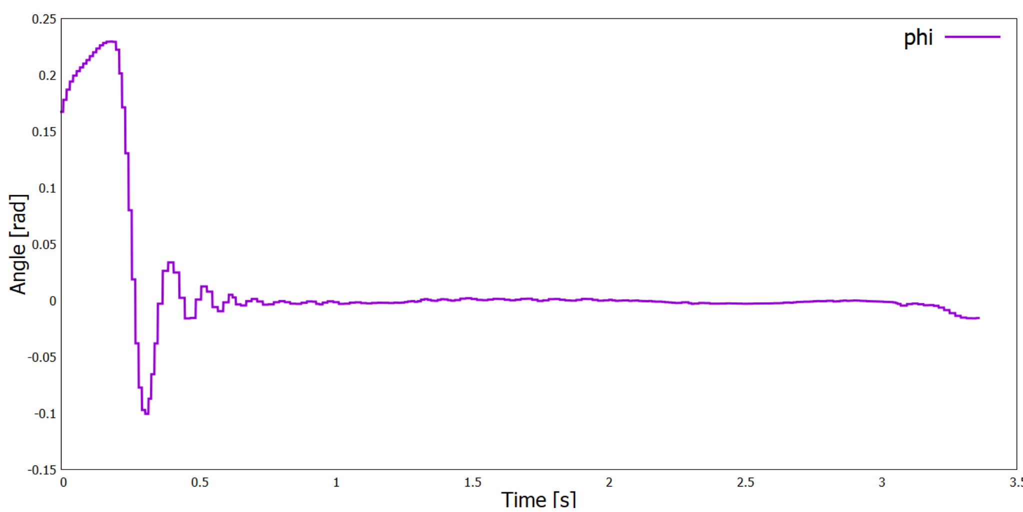

Figure 5.10: The angle of the two-wheeled walker in self-balancing.

The photos in Fig. 5.9 are caught from a recorded video with very small angle and position vibrations. These vibrations vary over the bend angle of the contact surface between the two-wheeled walker and the ground.

The two-wheeled walker is in strong self-balancing mode from 0.7 s to the end of the period without any vibrations with the initial point of 0.17 rad (Fig. 5.10).Thus, in the self-balancing mode, the effectiveness of the two-wheeled walker is verified. It is truly useful to assist the user to keep his balance.

5.3.2 Assist the User to Maintain Balance

a)

b)

Figure 5.11: New assistance types of the two-wheeled walker: (a) the whole body; (b) a half of the body.

The effectiveness of the two-wheeled walker will be proved when the whole body of the user is placed on it in this part (Fig. 5.11). Furthermore, the two-wheeled walker can go freely on the left and right sides banking on the actions of the user.

Fig. 5.12 reveals responses of the two-wheeled walker in two cases as shown in Fig. 5.11 to aid the user to stand, go forward and backward. In these cases, the user put two hands on two sides of the rod of the two-wheeled walker.

Banking on the evaluated force and the angle of the two-wheeled walker, the controller administers the walker to assist the user keep balance when the two-wheeled walker walks with the user. This is proved from the starting angle of 0.01 rad, the two-wheeled walker had a tiny vibration at around 0.2 s after power switched on. But, it approached the equilibrium position to assist the user keep balance while the whole body of the user was supported. Besides, it is easy for the user move forward or backward banking on the actions of the user' s hands. In detail, the walker supported the user to go ahead from 0.7 s to 0.9 s, and move backward from 1.0 s to 1.1 s as given in Fig. 5.12.

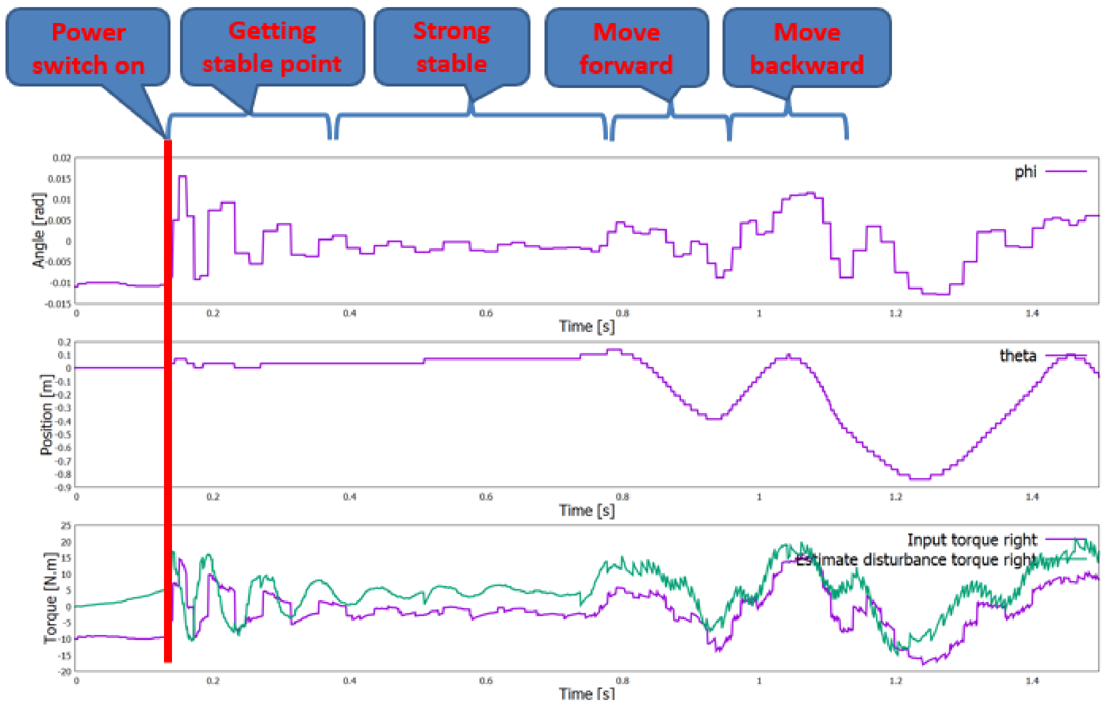

Figure 5.12: The position and the angle of the two-wheeled walker while aiding the user to walk.

Specially, in order to administer the movements of the two-wheeled walker, the human force estimation built on the nonlinear disturbance observer is utilized. The result in Fig. 5.13 reveals that when the user goes on the right or the left side, the estimated force is changed subsequently. Banking on this user' s actions, the controller can make the walker to assist the user turn on the right or the left better than other conventional methods.

When the input torque is put on the handle of the two-wheeled walker, the nonlinear disturbance observer evaluates the right and the left torques placed on the right and left handle of the user. Then, the two-wheeled walker is controlled to turn to the right or left side flexibly as illustrated in Fig. 5.13 corresponding to on the torque evaluated result.

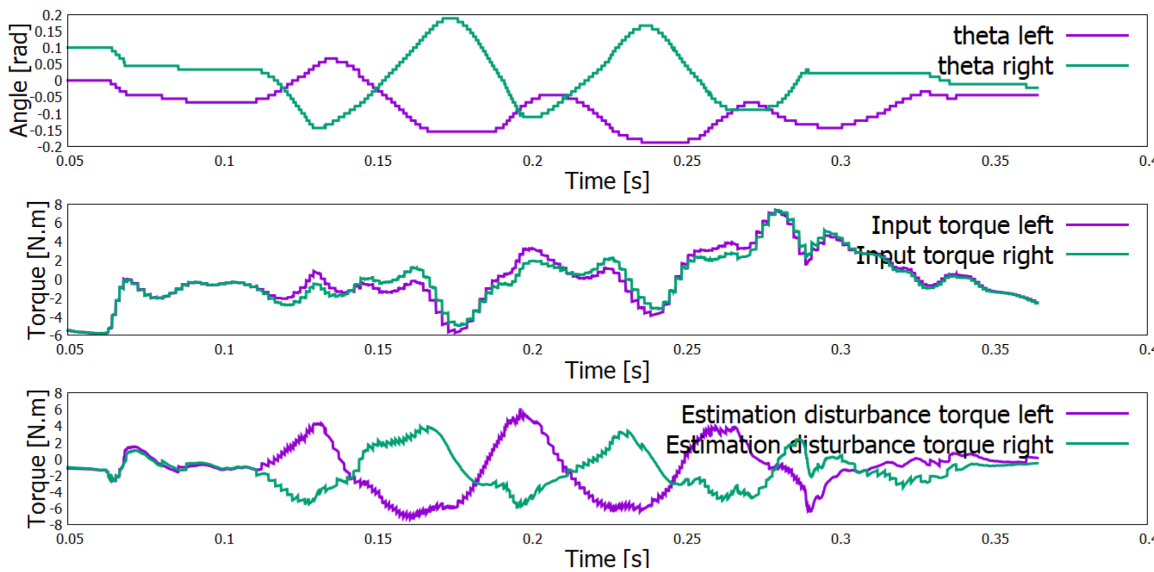

Figure 5.13: The angle and the torque of the two-wheeled walker while turning in measurement and estimation.

The results in the support mode were demonstrated that the two-wheeled walker is truly effective to assist the elder or the disabled to keep balance or to walk.

5.4 Smart Mode Switching Method

Fig. 5.14 on the top shows that the angle and the velocity of the rod of the two-wheeled cane is changed immediately when the rod varies.

The angle and velocity of the robot can be seen in the middle figure, by applying gain scheduling method to the nonlinear system, the two-wheeled cane can support the user switch modes immediately to help the elderly maintain balancing. Moreover, the estimated human force as shown in the bottom figure is also contributed to the successful operation of the robot.

Fig. 5.15 shows experimental results on robots with two instances of the central controller equipped with a low pass filter and without any low-pass filter. From on the top of the chart, it can be seen that when a low-pass filter is not used, this interference is quite large and almost occurs throughout the robot's working cycle. This interference disturbance is completely suppressed when a low-pass filter is utilized (the bottom graph of Fig. 5.15).

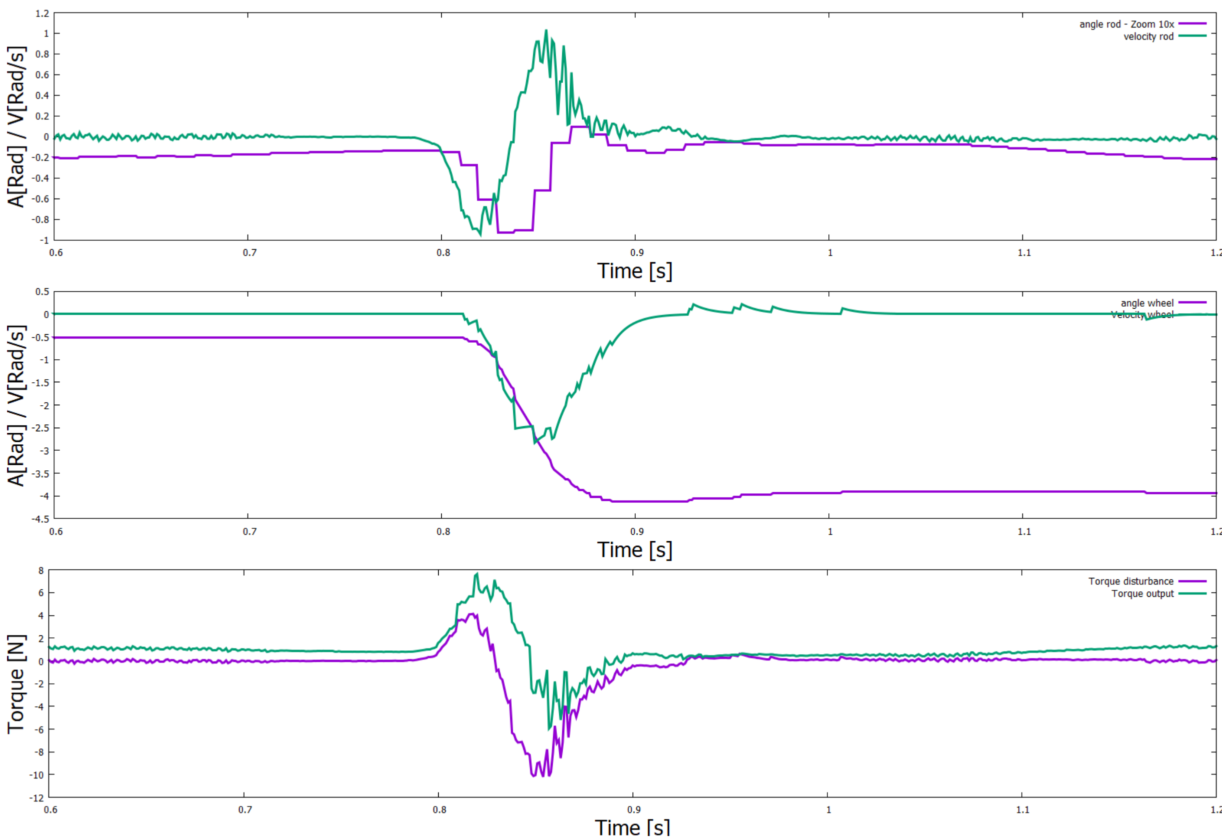

Figure 5.14: Response of the two-wheeled cane to the user's behaviors.

This interference oscillation arises when the pendulum model is inverted and to maintain equilibrium. To eliminate this interference, we recommend use a low-pass filter for signals into the controller's τ.

$$\tau_{current} = \alpha\tau_{current} + (1 - \alpha)\tau_{old} \tag{5.1}$$

with smoothing factor $0 \leq \alpha \leq 1$.

This control signal is directly affected by the movements of the motor through the controller. The α smoothing factor is chosen based on experiments for the specific robot model.

From these experimental results, the controller with a low-pass filter makes the user feel more comfortable while using the robot during the balancing and moving process. Smart mode switching can remove the vibrations when switching between two modes. The Low-pass-filter can suppress noises on the system. When these two methods are combined to control the motions of the robotic canes, the system support the user more smoothly.

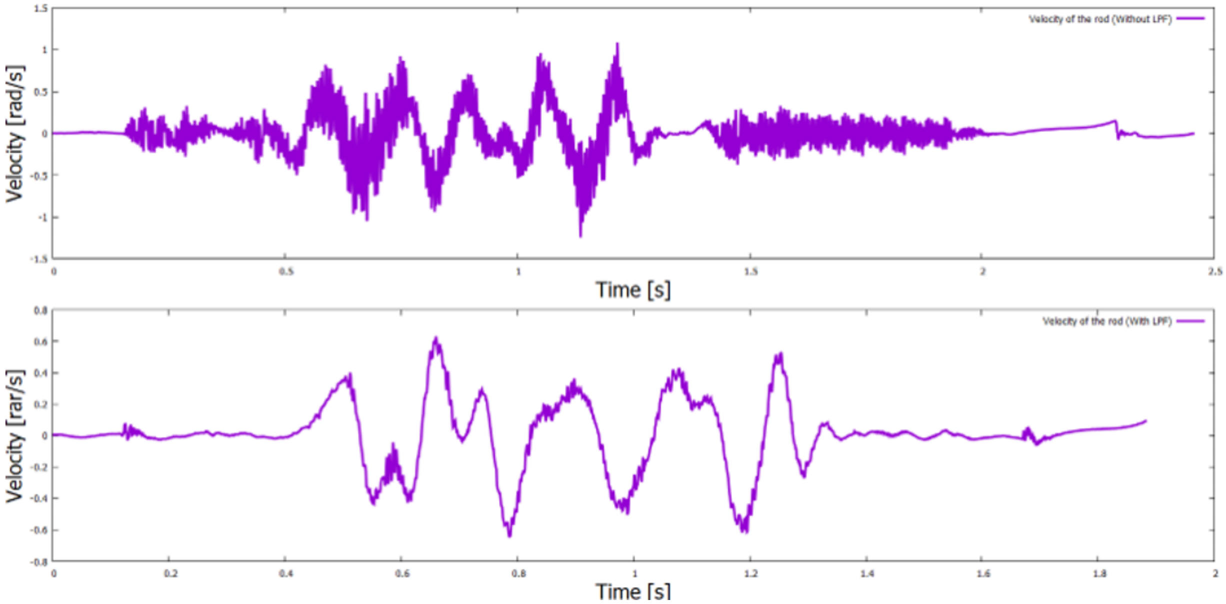

Figure 5.15: The two-wheeled cane is removed noises on the controller by utilizing the low-pass-filter.

5.5 Image Processing Application to Determine the Navigate Line of the Blind People

In this part, the experiment results of the application of image processing in recognizing the road for the blind will be discussed. Firstly, we test the program with some input pictures of the types of the navigate lines as shown in Fig. 5.16 (a) and Fig. 5.16 (b). Fig. 5.16 (a) shows that the color detection method can determine the navigate lines very clearly in indoor environments with the center gravity, the size, and the types of the lines by image comparison methods. Moreover, this method is also applied to the outdoor environments, and gives very good results same as the previous states as shown in Fig. 5.16 (b).

After finding the center of the navigate lines, a geometric image transformation method is used to transfer from the image coordinate system to the robotic cane coordinate system pre-

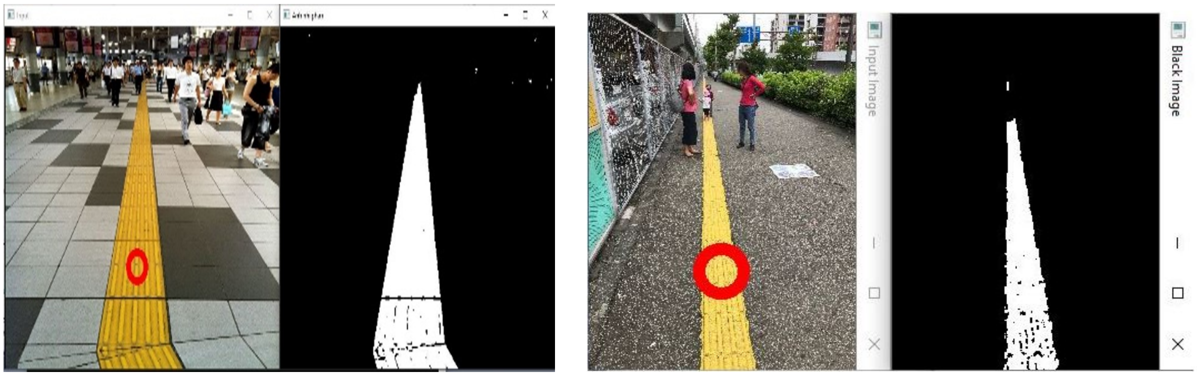

a) Indoor b) Outdoor

Figure 5.16: Image processing results to detect the straight line of the navigate lines.

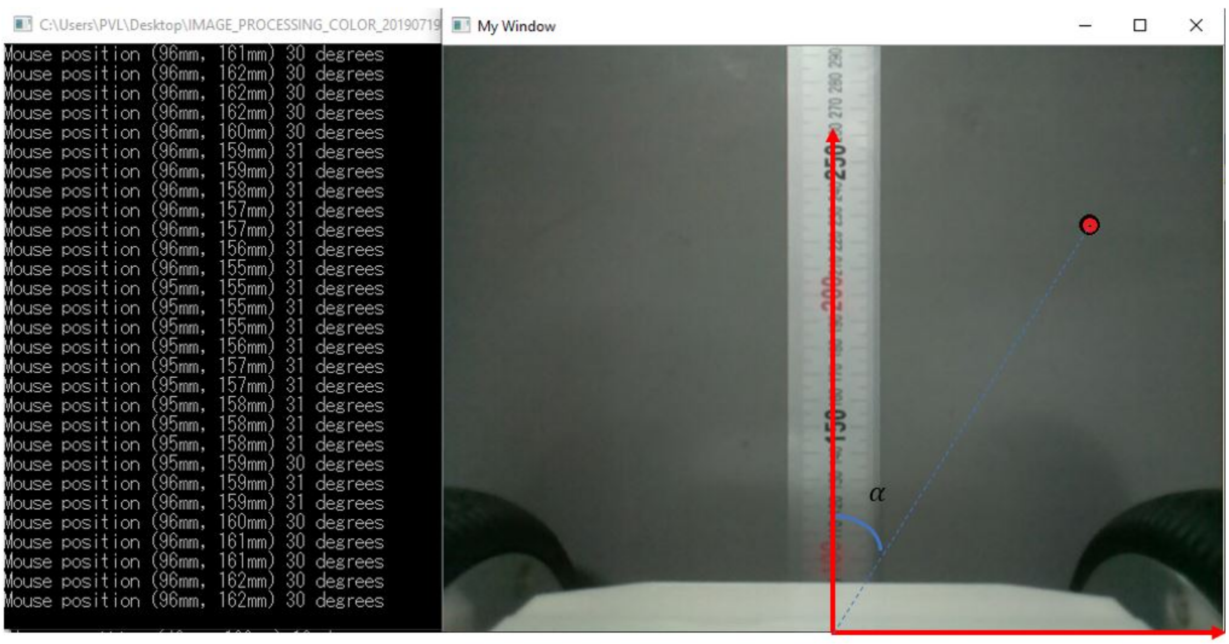

Figure 5.17: The angle α between the central gravity of the navigate lines and the head axis of the two-wheeled cane.

sented in the Chapter 3, which considered the error angle between the center gravity of the navigate lines and the head axis of the robotic canes.

Fig. 5.17 shows that by applying the geometric image transformation we can calculate the angle (α = 30 degrees) between the central gravity of the object and head axis of the two-wheeled cane. The α is used as a reference input variable to the PD controller.

From these results, it is admitted that the proposed center controller of the robotic canes can

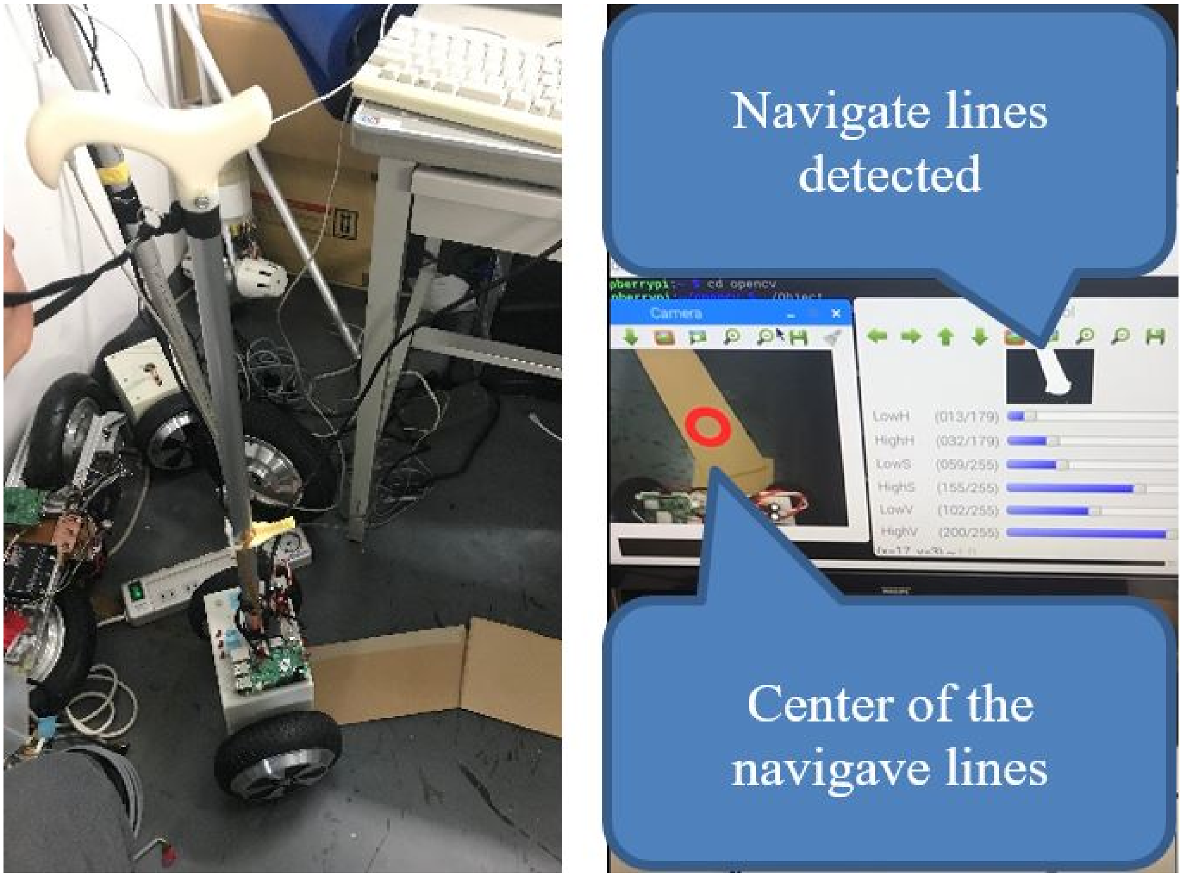

Figure 5.18: Tested image processing results with a indoor reference line on the body of the two-wheeled cane with the PD controller.

use the locations of the navigate lines of the image processing algorithms to control the motions of the robotic canes based on PD controller to help the user maintain balancing through α.

By using the image processing method, the center gravity of the navigate lines of the blind people is found as the right of Fig. 5.18. Then, the PD controller will control the motions of the robotic canes following the navigate lines while supporting the user maintain balancing.

5.6 Summary

In this chapter, we proved the performance of the LAM when it is applied to the nonlinear system including NDOB built on inverted pendulum models by the experiment results on the two-wheeled cane and the two-wheeled walker.

The stability of the system is indicated by the angle of the rod of the robotic canes which is close to the equilibrium point of the inverted pendulum model.

A new method - smart mode switching was proposed and applied to the controller of the robotic canes, which makes the application ability of the robotic canes to support the user to maintain balancing become much more practical compared with one gain to control the system as the traditional methods.

Moreover, from the experiments on slope environments, we are sure that our robotic canes will be put into application in practice in the near future to support the user to walk on any environments, that is impossible with the conventional devices for walking assistance.

Chapter 6

Conclusion

6.1 Summary

This chapter comes to an end, which summarizes addressed issues in this Thesis, highlights the main results. Firstly, the hardware of a robotic cane with an omnidirectional wheel was designed and fabricated. Then, two new types of the robotic canes: the two-wheeled cane and the two-wheeled walker are developed based on the first one. Two new models can support the user better than the original one.

In detail, the two-wheeled cane uses two natural rubber tire electric wheels containing brushless motors and hall sensors, and it can work smoothly without any vibrations. Next, the two-wheeled walker was designed with a U-shaped frame which can stand the whole bodyweight of the user, and therefore, it can support the user in more cases like the user can not stand properly. Interestingly, a camera combined with the image processing method is installed on the canes to support the blind find the navigate lines.

The center controller of the robotic cane is a Raspberry Pi 3 Model B+ computer built on the Raspbian OS for C/C++ coding for assisted standing and walking. The controller estimates the user's external force by a LAM-based linearization system with a nonlinear disturbance observer. In 3D simulations and physical tests of the robotic canes hardware, the robotic canes provided better balance maintenance support than previously proposed methods.

The proposed robotic canes proved an excellent candidate in various assistance modes: self-balancing, standing support, walking assistance, fall prevention, and a mechatronic safety mode. With the newly proposed method of smart switching modes, the robotic canes can help the users maintain balancing more convenience.

The Low-pass-filter applied to the controller of the robotic canes can remove the appearance of the noise on the experiment in real models. The combined smart switching mode and low-pass-filter to applied to the controller of the robotic canes to make more comfortable when helping the user maintain balancing.

Provide a new method applied to the robotic canes to support the blind people to walk by using image processing algorithms to determine the navigate line using color detection algorithm. Besides, bu using image processing method included PD controller was applied to the robotic canes are useful to support the blind people to maintain balancing while flowing the navigate lines without any problems as presented by the experiment results.

The evaluation of the performance of the methods applied to the actual model of the robotic canes is carried out on a variety of objects and different working environments give equally good results in walking assistance functions.

The robotic canes are expected as one of the smart walking assistance devices to support older or disabled persons included blind people in the near future of our smart social.

6.2 Future Work

In future work, we will reduce the size of the robotic canes and increase the working time of the batteries before recharging is required. We will then test a commercial version of the robotic cane in rehabilitation centers and hospitals.

Bibliography

[1] Chaio Shiung Chen and Wen Liang Chen. Robust adaptive sliding mode control using fuzzy modeling for an inverted pendulum system. *IEEE Transactions on Industrial Electronics*, 45(2):297–306, Apr 1998.

[2] Hiroaki Fukushima, Keiji Muro, and Fumitoshi Matsuno. Sliding mode control for transformation to an inverted pendulum mode of a mobile robot with wheel arms. *IEEE Transactions on Industrial Electronics*, 62(7):4257–4266, July 2015.

[3] John B. Morrell Hari Vasudevan, Aaron M. Dollar. Design for control of wheeled inverted pendulum platforms. *Journal of Mechanisms and Robotics*, 2015.

[4] Simon Hauser, Matthew Robertson, Auke Ijspeert, and Jamie Paik. Jammjoint a variable stiffness device based on granular jamming for wearable joint support. *IEEE Robotics and Automation Letters*, 2(2):849–855, April 2017.

[5] Yi Hung Hsieh, Kuu Young Young, and Chun Hsu Ko. Effective maneuver for passive robot walking helper based on user intention. *IEEE Transactions on Industrial Electronics*, 62(10):6404–6416, Oct 2015.

[6] Jian Huang, Zhi Hong Guan, Takayuki Matsuno, Toshio Fukuda, and Kosuke Sekiyama. Sliding mode velocity control of mobile wheeled inverted pendulum systems. *IEEE Transactions on Robotics*, 26(4):750–758, Aug 2010.

[7] Jian Huang, Songhyok Ri, Lei Liu, Yongji Wang, Jiyong Kim, and Gyongchol Pak. Nonlinear disturbance observer based dynamic surface control of mobile wheeled inverted pendulum. *IEEE Transactions on Control Systems Technology*, 23(6):2400–2407, Nov 2015.

[8] Alberto Isidori. Nonlinear control systems: An introduction. In *Third edition, Chapter 4: Elementary Theory of Nonlinear Feedback for Single-Input Single-Output systems, London, UK: Springer-Verlag*, 2001.

[9] Giho Jang, Junghoon Kim, Sungon Lee, and Youngjin Choi. Emg based continuous control scheme with simple classifier for electric powered wheelchair. *IEEE Transactions on Industrial Electronics*, 63(6):3695–3705, June 2016.

[10] Sunil K. Agrawal Kaustubh Pathak, JaumeFranch. Velocity and position control of a wheeled inverted pendulum by partial feedback linearization. *IEEE Transactions on Robotics*, 21(3), June 2005.

[11] Soo Yeon Kim, Li Yang, In Jae Park, Eun Joo Kim, Min Su Park, Sung Hyun You, Yun Hee Kim, Hyun Yoon Ko, and Yong Il Shin. Effects of innovative walkbot robotic-assisted locomotor training on balance and gait recovery in hemiparetic stroke: A prospective, randomized, experimenter blinded case control study with a four-week follow-up. *IEEE Transactions on Industrial Electronics*, 23(4):636–642, July 2015.

[12] Bram Koopman, Edwin H. F. van Asseldonk, and Herman van der Kooij. Estimation of human hip and knee multi joint dynamics using the lopes gait trainer. *IEEE Transactions on Robotics*, 32(4):920–932, Aug 2016.

[13] Phi Van Lam and Yasutaka Fujimoto. Building and test a controller of the robotic cane for walking assistance. In *The IEEJ International Workshop on Sensing, Actuation, Motion Control, and Optimization*, volume 3, pages SS2–6, March 2017.

[14] Phi Van Lam and Yasutaka Fujimoto. Completed hardware design and controller of the robotic cane using the inverted pendulum for walking assistance. *2017 IEEE 26th International Symposium on Industrial Electronics (ISIE)*, 19-21 June 2017:2163–5145, August 2017.

[15] Hyunglae Lee and Neville Hogan. Time varying ankle mechanical impedance during human locomotion. *IEEE Transactions on Neural Systems and Rehabilitation Engineering*, 23(5):755–764, Sept 2015.

[16] Jinfu Li, Bingquan Shen, Chee Meng Chew, Chee Leong Teo, and Aun Neow Poo. Novel functional task based gait assistance control of lower extremity assistive device for level walking. *IEEE Transactions on Industrial Electronics*, 63(2):1096–1106, Feb 2016.

[17] Chung Dial Lim, Chia Ming Wang, Ching Ying Cheng, Yen Chao, Shih Huan Tseng, and Li Chen Fu. Sensory cues guided rehabilitation robotic walker realized by depth image - based gait analysis. *IEEE Transactions on Automation Science and Engineering*, 13(1):171–180, Jan 2016.

[18] Mohammad Jawad Mahmoodabadi and S. Arabani Mostaghim. Stability of nonlinear systems using optimal fuzzy controllers and its simulation by java programming. *IEEE Journal of Automatica Sinica*, pp(99):1–10, Jan 2017.

[19] S. A. Hutchinson N. R. Gans. Visual servo velocity and pose control of a wheeled inverted pendulum through partial feedback linearization. *IEEE International Conference on Intelligent Robots and Systems*, October 2006.

[20] Shotaro Nakagawa, Yasuhisa Hasegawa, Toshio Fukuda, Izumi Kondo, Masanori Tanimoto, Pei Di, Jian Huang, and Qiang Huang. Tandem stance avoidance using adaptive and asymmetric admittance control for fall prevention. *IEEE Transactions on Neural Systems and Rehabilitation Engineering*, 24(5):542–550, May 2016.

[21] Luis Mario Lizarraga Orozco, Guillermo Ronquillo Lomeli, Jose Gabriel Rios Moreno, and Mario Trejo Perea. Identification inverted pendulum system using multilayer and polynomial neural networks. *IEEE Latin America Transactions*, 13(5):1569–1576, May 2015.

[22] Yasuhiro Ota, Masaru Ryumae, and Keiichi Sato. Robotic cane devices. https://patentimages.storage.googleapis.com/5a/f4/f5/e7b51348f01b94/US8418705.pdf.

[23] L. S. Qin, J. J. Hu, H. X. Li, and Wang Chen. Fuzzy logic controllers for specialty vehicles using a combination of phase plane analysis and variable universe approach. *IEEE Access*, 5(99):1579–1588, Jan 2017.

[24] Peng Shi, Huijiao Wang, and Cheng Chew Lim. Network based event triggered control for singular systems with quantizations. *IEEE Transactions on Industrial Electronics*, 63(2):1230–1238, Feb 2016.

[25] Kyohei Shimizu and Yasutaka Fujimoto. A robotic cane for walking support using two control modes. In *IEEJ International Workshop on Sensing, Actuation, Motion Control, and Optimization*, pages TT9–5, March 2016.

[26] Kyohei Shimizu, Smadi A. Issam, and Yasutaka Fujimoto. Examination of a control method for a walking assistance robotics cane. In *IEEE Industrial Electronics Society Annual Conference (IECON)*, pages 1968–1973, Oct 2014.

[27] Kyohei Shimizu, Smadi A. Issam, and Yasutaka Fujimoto. A robotic cane for walking assistance. In *IEEJ International Power Electronics Conference (IPEC)*, pages 1968–1973, May 2014.

[28] Kyohei Shimizu, Smadi A. Issam, and Yasutaka Fujimoto. Operation verification of cane type walking support robot in step and slope situation. In *IEEJ International Workshop on Sensing, Actuation, Motion Control, and Optimization*, March 2015.

[29] Issam Abed Smadi and Yashutaka Fujimoto. Nonlinear control of mechanical systems with application to monowheel robot. *Yokohama National University*, 2009.

[30] Richard Suzman and John Beard. Global health and aging. http://www.who.int/ageing/publications/global_health.pdf.

[31] Daniel Yang, Eric Sihite, Jeffrey M. Friesen, and Thomas Bewley. Design and control of a micro ball-balancing robot (mbbr) with orthogonal midlatitude omniwheel placement. *IEEE/RSJ International Conference on Intelligent Robots and Systems (IROS)*, September 2016.

[32] Haoyong Yu, Sunan Huang, Gong Chen, Yongping Pan, and Zhao Guo. Human robot interaction control of rehabilitation robots with series elastic actuators. *IEEE Transactions on Robotics*, 31(5):1089–1100, Oct 2015.

[33] Chi Zhu, Masashi Oda, Masayuki Suzuki, Xiang Luo, Hideomi Watanabe, and Yuling Yan. A new type of omnidirectional wheelchair robot for walking support and power assistance. *2010 IEEE International Conference on Intelligent Robots and Systems*, pages 6028–6033, Oct 2010.

Related Publications

Journal Papers

- Phi Van Lam, Yasutaka Fujimoto, “A Robotic Cane for Balance Maintenance Assistance”, *IEEE Transactions on Industrial Informatics*, Issue Date: JULY 2019, Volume: 15, Issue:7, On Page(s): 3998-4009, Print ISSN: 1551-3203, Online ISSN: 1941-0050, Digital Object Identifier: 10.1109/TII.2019.2903893.

- Phi Van Lam, Yasutaka Fujimoto, “Image Processing Application in Controlling the Robotic Cane to Support the Blind Maintain Balance When Moving”, *Measurement, Control and Automation, Vietnamese*, Volume: 22, Issue: 01, Accepted on August 16, 2019.

Conference Papers

- Phi Van Lam, Yasutaka Fujimoto, “A Robotic Cane Control System Based on Image Processing for Supporting the Blind People”, in proc. *Vietnam-Japan Science and Technology Symposium (VJST2019)*, HaNoi, Vietnam, May, 2019.

- Phi Van Lam, Yasutaka Fujimoto, “Examination of a Control Method for a Walking Assistance of Two-Wheeled Walker”, in proc. *IEEE 2019 International Conference on Mechatronics (ICM2019)*, Ilmenau, Germany, March, 2019.

- Phi Van Lam, Tomoyuki Shimono, Yasutaka Fujimoto, “Using a Nonlinear Disturbance Observer to Estimated the Human Force Applied to a Two-wheeled Cane For Walking Assistance”, in proc. *IEEE Industrial Electronic Conference(IECON2018)*, Washington D.C, October, 2018.

- Phi Van Lam, Yasutaka Fujimoto, “Two-wheeled walker for walking assistance”, in proc. *Vietnam-Japan Scientific Exchange Meeting (VJSE2018)*, Invited speaker, Sendai, Japan, September, 2018.

- Phi Van Lam, Yasutaka Fujimoto, “Two-Wheel Cane for Walking Assistance”, in proc. *EEJ Int. Power Electronics Conference (IPEC2018)*, 21H2-4, Niigata, Japan, May, 2018.

- Phi Van Lam, Yasutaka Fujimoto, “Completed Hardware Design and Controller of the Robotic Cane Using the Inverted Pendulum for Walking Assistance”, in proc. *IEEE International Symposium on Industrial Electronics (ISIE2017)*, EF-007862, Edinburgh, June, 2017.

- Phi Van Lam, Yasutaka Fujimoto, “Building and Test a Controller of the Robotic Cane for Walking Assistance”, in proc. *IEEJ International Workshop on Sensing, Actuation, Motion Control, and Optimization (SAMCON2017)*, SS2-6, Nagaoka, Japan, March, 2017.

Honors & Awards

- Special Award (17th Intelligent Electronics (IE) Competition) held in July 2, 2019 Power Electronics Annual Conference, South Korea, Ref. No. IE19-6, Title of work: A Two-wheeled cane for walking assistance.